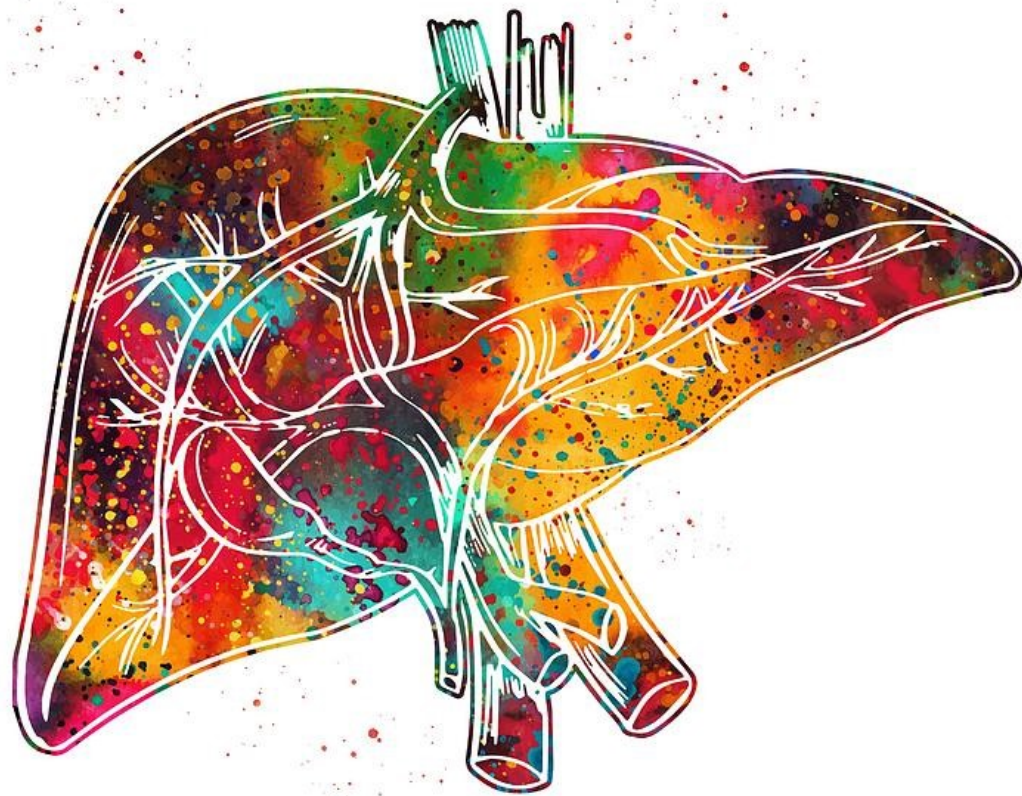# Intravoxel Incoherent Motion and Dynamic Contrast Enhanced Quantitative Magnetic Resonance Imaging in the Preoperative Evaluation of Liver Function

Technical Medicine master thesis project
Amsterdam University Medical Center, Delft University of Technology, Leiden University, Erasmus University Rotterdam

Fenna van der Zijden

August 2024

Intravoxel Incoherent Motion and Dynamic Contrast Enhanced Quantitative Magnetic Resonance Imaging in the Preoperative Evaluation of Liver Function

- Final report -

Fenna van der Zijden

4484665

15 August 2024

Thesis in partial fulfilment of the requirements for the joint degree of Master of Science in

Technical Medicine

Leiden University ; Delft University of Technology ; Erasmus University Rotterdam

Master thesis project (TM30004 ; 35 ECTS)

Dept. of Biomechanical Engineering, TUDELFT
Start project: 01-03-2024
Reportissued: 16-08-2024
Defensedate: 30-08-2024

Supervisor(s):
Dr. F.M. Vos, technical supervisor
O.J. Gurney Champion, technical supervisor
Dr. J.I. Erdmann, medical supervisor
P.J. Arntz, daily medical supervisor
B. Ariens, daily technical supervisor

Thesis committee members:

Dr. F.M. Vos, TU Delft (chair)
Dr. J.I. Erdmann, Amsterdam UMC
Dr. M.G.J. Thomeer, Erasmus MC

Universiteit Leiden   TUDelft Delft University of Technology   ERASMUS UNIVERSITEIT ROTTERDAM

Summary

Background: Surgical removal of liver tumors necessitates a thorough preoperative assessment to ensure adequate future liver remnant function, which is crucial for hepatic regeneration. Imaging techniques like hepatobiliary scintigraphy (HBS) and dynamic contrast-enhanced (DCE) magnetic resonance imaging (MRI) assess liver function by measuring the uptake of liver-specific contrast agents. Intravoxel incoherent motion (IVIM)-MRI measures both molecular diffusion and perfusion-related motion of water molecules in the liver. This provides valuable insights into tissue microenvironment changes that can indicate liver dysfunction. However, the potential of IVIM-MRI in this context remains unexplored. This study aims to evaluate the feasibility of IVIM-MRI for liver function assessment and its relationship with DCE-MRI. *Methods:* Twenty-one patients scheduled for major hepatectomy underwent preoperative assessment involving HBS, a 20-minute DCE-MRI series, and IVIM-MRI with 15 b-values. DCE-MRI parameters (hepatocyte uptake K_i(min^{-1}), arterial plasma flow F_a (mL/min/100 mL), and venous plasma flow F_v (mL/min/100 mL)), were analyzed using the Sourbron model. IVIM-MRI parameters (diffusion D (mm^2/s), pseudo-diffusion D_p (mm^2/s), and perfusion fraction f (%)) were extracted using a UNET model developed at Amsterdam University Medical Centers. Correlation between parameters was assessed using Pearson correlation analysis. Furthermore, Blant-Altman was employed to assess the inter-observer variability and the reproducibility of the DCE-MRI parameters. *Results:* In 19 patients, weak correlations were observed between DCE- and IVIM-MRI parameters, with correlation coefficients ranging from $r = -0.326$ to $r = 0.443$. Despite the lack of significant correlations between these parameters, strong correlations were observed between DCE-MRI K_i and HBS ($r = 0.80$, $p < 0.001$). Moreover, DCE-MRI parameters demonstrated high reproducibility, with Bland-Altman mean biases ranging from -1.79 to -0.08. *Conclusion:* The weak correlation observed between DCE- and IVIM-MRI parameters suggests that IVIM-MRI may have limited utility in preoperative liver function assessment. Nevertheless, DCE-MRI may serve as an alternative to HBS, potentially providing a one-stop shop for preoperative liver assessment with MRI. Further research is necessary to explore its potential in diverse populations with varying liver function.

Keywords: *quantitative magnetic resonance imaging, liver function, hepatectomy*

List of Abbreviations:
CLD - Chronic Liver Disease
HCC - Hepatocellular Carcinoma
PHLF - Post Hepatectomy Liver Failure
FLR - Future Liver Remnant
HBS - Hepatobiliary Scintigraphy
^{99m}Tc - Technetium-99m
MRI - Magnetic Resonance Imaging
CT - Computed Tomography
DWI - Diffusion Weighted Imaging
IVIM - Intravoxel Incoherent Motion
Gd-EOB-DTPA/Primovist - Gadolinium-ethoxybenzyl-diethylenetriamine pentaacetic acid
DCE - Dynamic Contrast Enhanced
K_i - Hepatic uptake rate
F_a - Arterial plasma flow
F_v - Venous plasma flow
T_f - Total plasma flow
f_a - Arterial flow fraction
D - True diffusion coefficient
D_p - Pseudo-diffusion coefficient
f - Perfusion fraction
TIC - Time Intensity Curve
AIF - Arterial Input Function
VIF - Venous Input Function
ROI - Region of Interest
MUR - ^{99m}Tc-mebrofenin Uptake Rate
TLF - Total Liver Function

Introduction

2.1 The liver

The liver is a vital organ responsible for many essential functions, including the regulation of metabolic processes, immunity, digestion, detoxification, and the storage of vitamins and other nutrients[1]. In addition, the liver has the capability to regenerate, as hepatocytes can proliferate, enabling the liver to restore and regain function after injury[2]. Anatomically, the liver is located in the upper right quadrant and is subdivided into eight independent segments by the Couinaud classification (Fig. 1a and 1b). The branches of the portal vein subdivide the liver horizontally into two parts, while the branches of the hepatic veins divide the liver vertically into four sections. Each segment is supplied by an individual Glissonian pedicle, which consists of a branch of the hepatic artery, the portal vein, and the bile duct[3].
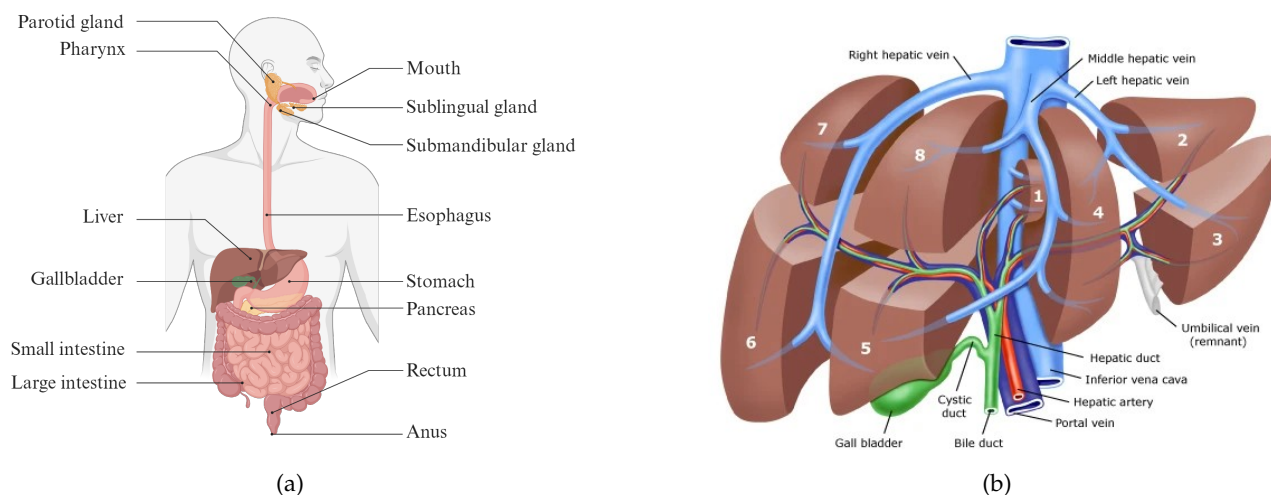

Figure 1: (a) Digestive system with the liver located in the upper right abdomen (b) Couinaud segments.

2.2 Liver diseases

The incidence of chronic liver disease (CLD) has increased dramatically over the past few decades, presenting a significant global health concern. This increase is attributed to several factors, such as the higher prevalence of viral infections like hepatitis B and C, rising rates of obesity and metabolic syndrome, widespread alcohol consumption, and an aging population[4]. Typically, CLD progresses through stages beginning with steatosis, inflammation and fibrosis, which can ultimately result in cirrhosis. Steatosis is defined as the pathological accumulation of fat within hepatocytes, which can lead to cellular dysfunction and inflammation. This can lead to hepatomegaly and impair metabolic functions. If left untreated, it may progress to fibrosis. This progression is driven by the activation of hepatic stellate cells into proliferative myofibroblasts, leading to excessive deposition of extracellular matrix. The resulting accumulation of extracellular matrix disrupts liver architecture, obstructs blood flow, and contributes to the progression of CLD into the irreversible stages of cirrhosis and hepatocellular carcinoma (HCC)[5, 6, 7]. HCC is the most prevalent primary liver malignancy. Besides primary liver malignancies, the liver is a common site for secondary malignancies[8]. Moreover, the biliary tract, which connects the liver to the intestines can be affected by cancers such as cholangiocarcinoma[9].

2.3 Liver treatment options

Treatment of liver disease and malignancies is dependent on the underlying etiology and stage. Early-stage CLD is often managed with lifestyle modifications and medication to prevent the progression of fibrosis. In contrast, liver malignancies, including primary, secondary and biliary tract tumors often may require interventions such as chemotherapy, radiotherapy, or surgical procedures. Local treatments, including ablation and resection, are the only curative options and provide the highest probability of long-term survival for patients with primary and secondary liver tumors. Surgery is recommended when radical excision with tumor-free margins is possible. Nevertheless, surgical removal carries significant risks, including post hepatectomy liver failure (PHLF), with mortality rates up to 18%[9]. For this reason, a comprehensive preoperative assessment is essential

for determining patient suitability and ensuring adequate future liver remnant (FLR) volume and function.

2.4 Preoperative liver assessment

In patients with assumed healthy livers, a standardized volume of 20-30% is generally considered sufficient. However, smaller liver remnant volumes are associated with an increased risk of hepatic dysfunction and postoperative complications. Moreover, in patients with steatosis, fibrosis or injury from drugs or chemotherapy, the hepatic function and regenerative capacity of the liver may be diminished due to the architectural disruption of the liver tissue (Fig. 2)[10, 11]. Therefore, for these patients functional assessment is required. Methods of assessing liver function include the indocyanine green clearance test and the ^{13}C-methacetin breath test[11]. However, these have limitations in assessing regional liver function and may not always correlate with the true functional capacity of the remnant liver. To address these limitations, advanced imaging techniques, including Technetium-99m (^{99m}Tc)-mebrofenin hepatobiliary scintigraphy (HBS) and Magnetic Resonance Imaging (MRI) have emerged as promising alternatives[11].
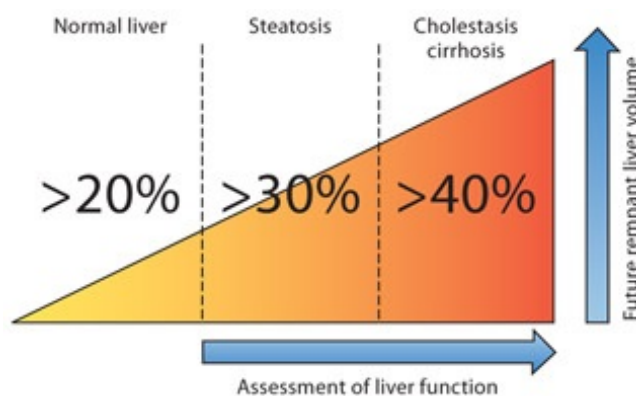

Figure 2: The diagram illustrates the minimum future liver remnant volumes required for safe liver resection based on underlying liver disease. Accurate liver function assessment is essential to determine the appropriate future liver remnant volume for ensuring postoperative safety.

2.5 Hepatobiliary scintigraphy

HBS has been developed for the assessment of total and regional liver function, employing radiotracers to measure hepatic uptake and excretion. The radiotracer ^{99m}Tc-mebrofenin is taken up from the blood through organic anion transporting polypeptides into hepatocytes and subsequently excreted through the bile ducts and gallbladder. As the radiopharmaceutical travels through the body, it emits gamma rays, which are captured by a gamma camera. When hepatocyte function is impaired in specific regions, these areas appear darker due to reduced excretion. HBS is used as standard of care in many centers to assess the risk of PHLF-related complications in patients undergoing major liver surgery. This risk increases when FLR function is below the cut-off value of 2.7%/min[12]. HBS has been shown to be effective in predicting PHLF. However, it focuses on hepatocyte uptake capacity, without assessing other indicators of liver disease that may impact liver function. Moreover, due to its limited spatial resolution, there is a necessity to provide an anatomical reference with a low-dose computed tomography (CT) imaging[13]. Alternatively, MRI has been suggested as a potential one-stop shop examination for preoperative planning of hepatectomy due to integration of anatomical imaging and its potential to measure function as well (Appendix D).

2.6 Magnetic resonance imaging

MRI employs a magnetic field to align the hydrogen nuclei present in body tissues. Radiofrequency pulses are applied to excite nuclei, thereby causing them to transition to a higher energy state. Following the application of the radiofrequency pulse, the nuclei emit radiofrequent signals as they return to their equilibrium states. A T1 image represents the degree to which the magnetization has returned to equilibrium following a period of time, whereas a T2 image represents the amount of magnetization that remains in the excited state after a period of time. Differences in relaxation times between tissues create contrast in images. Diffusion weighted imaging

(DWI) assesses the Brownian motion of water molecules. Variations in the organization and structure of liver parenchyma affect the diffusion coefficient of water, providing image contrast. T1, T2 and DWI sequences provide anatomical information of soft tissue, tumor, vascular structure, and anatomy[14].

However, these MRI sequences provide complementary signals in arbitrary units as pixel intensities. To extract functional information from these signals, several quantitative MRI techniques have been developed. For example, by measuring the DWI signal at various diffusion weightings, the apparent diffusion coefficient can be computed, offering valuable insights into tissue characteristics. Additionally, bi-exponential analysis using intravoxel incoherent motion (IVIM)-MRI helps to distinguish between perfusion-related and diffusion-related components[15].

T1-relaxometry, combined with liver-specific contrast agents such as Gadolinium-ethoxybenzyl- diethylenetri-amine pentaacetic acid (Gd-EOB-DTPA; Primovist®), is employed to assess hepatocyte capacity for contrast agent uptake. By measuring differences in signal intensity or relaxation rate during the arterial and hepatobiliary phases, liver function can be evaluated[16]. Moreover, dynamic contrast enhanced (DCE)-MRI assesses hepatobiliary function by monitoring the dynamics of a hepatocyte-specific contrast agent over time. Pharmacokinetic models are then employed to compute parameters such as permeability, flow, and hepatocyte excretion[17].

2.7   Rationale

DCE-MRI has demonstrated correlations with traditional liver function tests, including the indocyanine green clearance test and HB S[18, 19, 20]. Nevertheless, DCE-MRI is limited by its reliance on contrast agents and complexity in acquisition and post-processing. Complementary, IVIM-MRI offers information on microcirculation and molecular diffusion without the need for contrast agents[21]. As liver fibrosis affects perfusion and cell density, IVIM-MRI has the potential to offer valuable insights into hepatic function. Phonlakrai et al. demonstrated moderate correlations between IVIM-MRI parameters and hepatic uptake fraction in patients undergoing radiation therapy[22]. Additionally, Hectors et al. reported correlations between DCE- and IVIM-MRI parameters in the liver parenchyma of patients with HCC[23]. However, to date, no studies have investigated the degree to which IVIM-MRI correlates with DCE-MRI and HBS in patients scheduled for major hepatectomy.

Therefore, the aim of this study was to explore the feasibility of IVIM-MRI in assessing liver function and its relationship to DCE-MRI in the evaluation of liver function before hepatectomy. By considering alternative aspects of liver perfusion and diffusion with IVIM-MRI, liver function may be assessed more comprehensively. We hypothesize that DCE- and IVIM-MRI parameters will correlate, as both techniques measure aspects of liver diffusion and perfusion. A correlation between the DCE-MRI hepatic uptake rate (K_I) and the diffusion coefficient (D) was expected because both parameters are influenced by the tissue microenvironment, which affects molecular mobility. Furthermore, a correlation was expected between the arterial and venous plasma flows (F_A and F_V) from DCE-MRI and the pseudo-diffusion coefficient (D_p) from IVIM-MRI, as both parameters are influenced by microvascular blood flow. As a secondary objective, repeated analysis was conducted to assess the inter observer variability of the DCE-MRI measurements and their correlation with HBS.

Methods

3.1   Patients

This internal validation study used the dataset derived from a study comparing HBS and DCE-MRI, encompassing patients from the Amsterdam University Medical Centers during the period from December 2014 to July 2018[18]. Inclusion criteria were adult patients (age above 18 years) diagnosed with one or more liver lesions scheduled for major hepatectomy. Exclusion criteria included patients with contraindications to MRI, chronic renal impairment or history of congenital prolonged QT-syndrome, arrhythmia after the use of cardiac repolarization time prolonging drugs, bronchial asthma and allergies to gadolinium. The principle investigator from the previously conducted study by Rassam et al. approved reuse of the dataset and extended on the informed consent given. The study was registered at Amsterdam University Medical Centers under ID NL45755.018.13.

3.2 Image acquisition

Patients scheduled for major hepatectomy received ^{99m}Tc-mebrofenin and underwent DCE- and IVIM-MRI, within two weeks of the surgery.

3.2.1 HBS

A dual-head SPECT-CT camera (Siemens Symbia T16) with low-energy high-resolution collimators was used for acquisition. The energy window was 140 KeV. The dynamic acquisition started immediately after the intravenous bolus injection of the radiopharmaceutical ^{99m}Tc-mebrofenin (200 MBq; 5.41 mCi, Bridatec, GE Healthcare). Two dynamic acquisitions were conducted to measure the hepatic uptake and biliary excretion phases. Acquisition settings included 38 frames of 10 seconds per frame in a 128 × 128 matrix size for the uptake phase. In the biliary excretion phase 15 frames of 60 seconds per frame in a 128 × 128 matrix size were used. After the first dynamic acquisition, a SPECT imaging (60 projections of 8 seconds per projection, 128 × 128 matrix) combined with low-dose CT imaging was performed. This combination was used as an anatomical reference and for attenuation correction.

3.2.2 DCE- and IVIM-MRI

DCE images were acquired on a Philips 3.0 Tesla Ingenia MR scanner (Philips Healthcare). T1-weighted gradient echo DCE images were acquired in the axial orientation. Scanning parameters included a 15 degree flip angle, 2.30 ms echo time, 3.75 ms repetition time, 3x3x5 mm^3 voxel size and 128x128x44 matrix size. The DCE-MRI protocol consisted of four acquisition phases (0 s, 22 s, 3 min, 12 min), spread out over 20 minutes. After the first acquisition, a bolus of Primovist contrast agent was injected (0.1 mL/kg). Sampling intervals during the first two acquisitions were 2.2 s, while a sampling interval of 30 s and 60 s was used for the third and fourth acquisition phases, respectively. Increasingly higher values were used as the uptake of contrast slows down over time. This resulted in 108 volumes in total. For IVIM-MRI, a multi-slice diffusion-weighted single shot echo-planar imaging sequence with multiple b-values (0, 1, 2, 4, 6, 9, 12, 17, 24, 37, 54, 98, 147, 220, 294 mm²/s) was used. IVIM images were acquired in the coronal orientation. Parameters for the sequence included a 56 ms echo time, 3.9 ms repetition time, a 3.5x3.5x5 mm^3 voxel size and 80x80x25 matrix size.

3.3 Image analysis

3.3.1 HBS

The Hermes software platform (Hermes Medical Solutions) was used for image analysis. Image analysis was performed in line with the joint EANM/SNMMI/IHPBA HBS procedure guideline[24]. Signal attenuation correction was applied to address differences in signal intensity between the anterior and posterior datasets by computed the geometric mean of both datasets. The first step in post-processing was to identify the starting point, defined as the first image in the hepatic uptake phase with inflow of the radiopharmaceutical in the aorta. All images prior to this point were discarded. Regions of interest (ROIs) were then defined. The ROI for the blood pool was manually delineated on the initial image by defining the boundaries of the left ventricle and the aortic root (Fig. 3a). The liver ROI was defined semi-automatically using a threshold based approach (Fig 3c). The field of view was employed as the third ROI for the computation of the total body activity. The FLR was manually delineated on the SPECT-CT images, based on the planned resection (Fig. 3b). The liver ROI was employed to compute the ^{99m}Tc-mebrofenin uptake rate (MUR; %/min), which was defined by equation:

$$\text{MUR} = \frac{L(t_2) - L(t_1)}{A(t_1) \int_{t_1}^{t_2} C_{\text{norm}}(t)\, dt} \tag{1}$$

where $L(t_2) - L(t_1)$ represents the change in liver activity between the time points t_1 and t_2, $A(t_1)$ is the total activity in the blood pool at the initial time point t_1, and $\int_{t_1}^{t_2} C_{\text{norm}}(t)\, dt$ is the normalized concentration of the radiotracer in the blood over the time interval[25]. The total liver function (TLF) was defined as the percentage of radio tracer that has accumulated in the liver over a certain period of time. The functional share of the FLR was defined as the ratio of the FLR counts to the total liver counts measured in SPECT-CT volumes. The FLR function was then computed by multiplying this functional share by the total liver MUR.
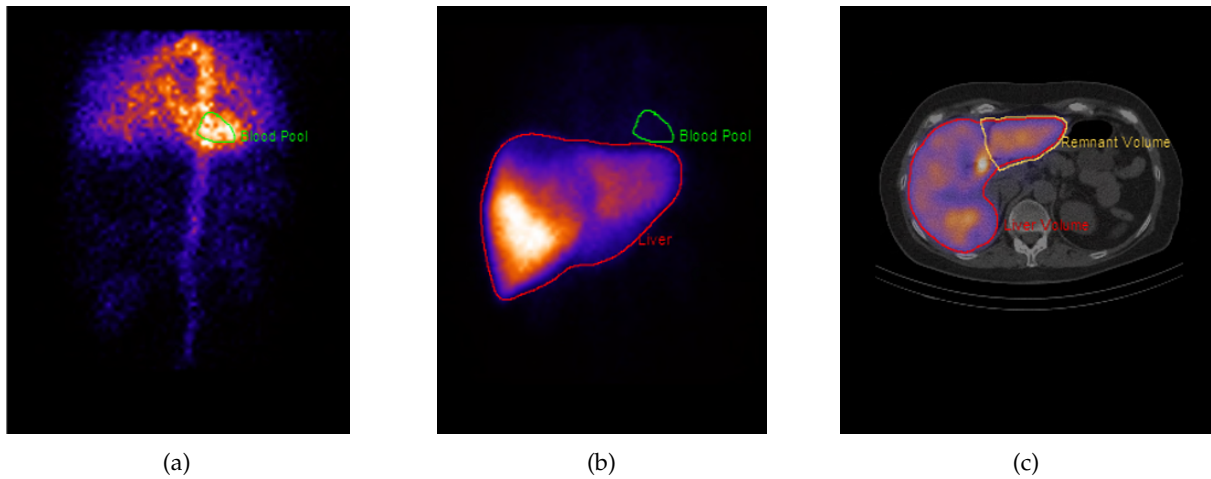
Figure 3: HBS postprocessing steps in the Hermes software platform: (a) Manual delineation of the blood pool and aortic root, (b) semi-automatic delineation of the liver, (c) manual delineation of the future liver remnant volume.

3.3.2 DCE

The analysis of DCE-MRI data in our study involved several steps: 1) pre-processing; 2) extraction of time intensity curves (TICs); 3) conversion to gadolinium concentration; 4) application of Orton's model to analytically represent the vascular input functions[26]; and 5) use of Sourbron's model to estimate biological parameters from the fitted data[27].

The modality independent neighborhood descriptor method was employed to register the DCE images over time. This method employs a pixel neighborhood approach, focusing on image structures for image registration rather than signal intensities. This renders it particularly useful for contrast-enhanced images. The last time frame was selected as the reference image, as the liver is enhanced with contrast in this time frame. Automatic segmentation of the aorta and a manually delineated ROIs of the portal vein were employed at peak TIC to determine the arterial input function (AIF) and venous input function (VIF). Subsequently, voxel-based TICs were extracted from both regions and normalized. A mean TIC for both AIF and VIF were computed from the three individual curves with the greatest contrast enhancement. TICs were converted into plasma concentration by taking into account the flip angle, repetition time, native T1-relaxation times, Primovist relaxivity and hematocrit concentration. A hematocrit value of 0.46 and a contrast agent relaxivity value of 7.3 L/s/mmol were used[28, 29]. A modified Orton's model was used to analytically derive the AIF input function[30]. If patient-based VIF and AIF computation was not possible (e.g., due to early contrast inflow), population-based AIF and VIF were applied. The population-based AIF and VIF were derived by fitting parameters from all individual curves within the study cohort. First, the median of these fitting parameters was computed. Then, a population based curve was generated by fitting the median parameters. In the last step, the Sourbron pharmacokinetic model was applied (Fig. 4). This is a dual-inlet, two-compartment model that represents the physiological structure of the liver and was specifically designed for the Primovist contrast agent[27]. Extracted parameters were the arterial and venous plasma flows (F_a, F_v (mL/min/100mL)) and the hepatic uptake rate (K_i (min^{-1})). Besides the computed parameters, the total in-flow ($T_f = (F_a + F_v)$(mL/min/100mL)) and the arterial flow fraction ($f_a = (F_a/F_a + F_v)$(%)) were derived. These parameters reflect the balance between arterial and venous contributions, which may shift in response to underlying liver disease[31].
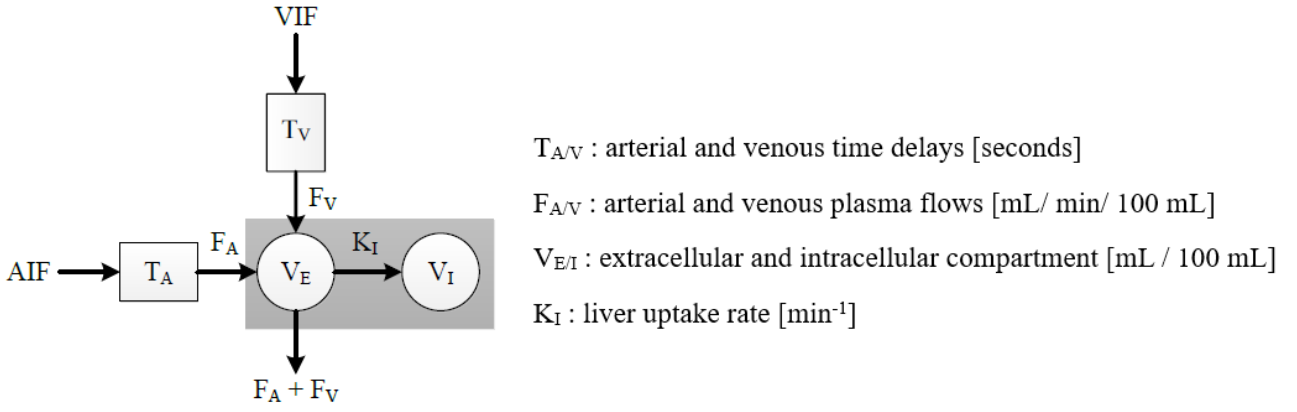
Figure 4: The Sourbron dual compartment dual inlet model employed in DCE-MRI with Primovist for analyzing tissue perfusion and permeability. The gray rectangle represents the liver. AIF, Arterial Input Function; VIF, Venous Input Function.

3.3.3 IVIM

ITKsnap Version 3.8.0 (US National Institutes of Health) was employed to perform image post-processing[32]. Manual segmentation of the liver was performed in ITKsnap with a threshold based region growing approach. The resulting segmentation was used for image registration. To align the 4D image dataset across different b-values, affine image registration was performed using Elastix for MATLAB. Principle component analysis and maximum intensity projection were applied to minimize artifacts and enhance signal to noise ratio.

Image analysis was performed in the Python programming language within the PyTorch environment. Images were transformed for analysis by converting them from 4D to 2D arrays, representing each voxel across all b-values. Data normalization was performed using the zero b-value as a reference. Subsequently, a publicly available IVIM UNET was employed to estimate IVIM-MRI parameters (D (mm^2/s), D_p (mm^2/s), f (%))[33, 34]. The IVIM model was described by the formula:

$$S(b) = S_0 \left(f \cdot e^{-bD_p} + (1 - f) \cdot e^{-bD} \right) \tag{2}$$

where $S(b)$ is the signal intensity at a given b-value (b), S_0 is the signal intensity without diffusion weighting ($b = 0$), D is the true diffusion coefficient, D_p is the pseudo-diffusion coefficient, and f is the perfusion fraction. The neural network was trained on an image array comprising all patients to estimate these parameters. After training, the same neural network was applied to estimate the IVIM-MRI parameters for each patient separately.

3.4 DCE- and IVIM-MRI parameter extraction

DCE and IVIM images were acquired in different orientations (axial and coronal). Consequently, rigid registration was applied to align the images and facilitate voxel-wise comparison within ROI. Due to the superior spatial resolution of the DCE images relative to the IVIM images, the IVIM images were registered to the DCE images. Automatic segmentation of the entire liver, along with manual delineation of the FLR, was performed on the DCE-MRI K_i map. Additionally, a standardized approach for ROI-based measurements was employed to extract data from the Couinaud liver segments[35]. Binary masks were generated from the segmentations and overlaid on the DCE-MRI K_i, F_a, F_v parametric maps as well as on the IVIM-MRI D, D_p, and f parametric maps. Within the entire liver and the FLR delineation, the sum values of K_i were computed to determine the functional share of the FLR. FLR function values were calculated by multiplying the functional share with the mean K_i of the FLR.
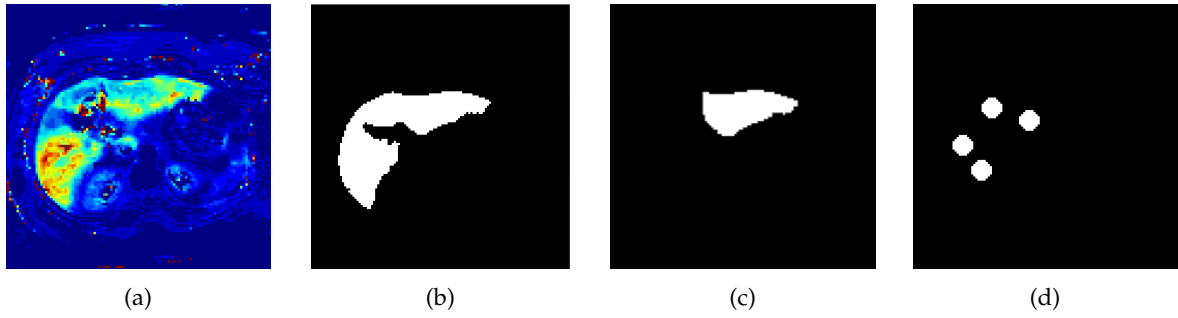
Figure 5: DCE-MRI K_i parametric map and corresponding masks of patient 19. (a) K_i parametric map, (b) entire liver mask, (c) FLR mask, (d) ROI mask of 4 mm^2 on the Couinaud segments at the level of the splenic vein.

3.5   Histological analysis

The intraoperative liver biopsy of the future remnant liver was performed by the operating surgeon, according to the standard of care for regular (i.e., non-research) intraoperative liver biopsies. Approximately 1 cm^3 of liver tissue was removed for all patients. The degree of fibrosis in the resected liver was computed based on the METAVIR scoring system by a pathologist.

3.6   Statistical analysis

Statistical analysis was conducted using SPSS. The minimum and maximum values, mean, and standard deviation range were calculated for the extracted DCE- and IVIM-MRI parameters. Correlations between DCE- and IVIM-MRI parameters, as well as between DCE-MRI parameters and HBS results, were analyzed using the Pearson correlation analysis. Additionally, the same correlation analysis were used to evaluate the relationships between derived IVIM-MRI parameters and histological parameters. P-values less than 0.05 were considered to indicate statistical significance. In order to evaluate the reproducibility of DCE-MRI parameters and assess agreement with previously published results, a Bland-Altman analysis was conducted on corresponding data sets from the same patients. Furthermore, agreement between functional share values measured on DCE-MRI and HBS was assessed using the same analysis.

Results

4.1 Patient characteristics

A total of 21 patients were scanned; two were excluded from the study due to protocol violations, one patient did not receive Primovist, and the MRI scan for a different patient was terminated at the patient's request. Histological data was not available for four patients; two of these patients did not undergo surgery, and two did not receive a FLR biopsy. All included patients underwent HBS and MRI within a two-week interval. Histological analysis demonstrated that 12 of the patients were classified as F0, four as F1, two as F2, and one as F4 according to the METAVIR scoring system. Patients with METAVIR score above F0 had HCC, intrahepatic cholangiocarcinoma or benign liver tumors. Five patients received neoadjuvant chemotherapy; however, no chemotherapy-associated liver injury was observed. Patient characteristics are summarized in Table 1.

4.2 Image processing

4.2.1 HBS

The image analysis was successfully conducted using the Hermes software platform in accordance with the procedural guidelines. Average values of the TLF and FLR are displayed in Table 2.

4.2.2 DCE

DCE-MRI images were processed using the described methodology (Appendix A). TICs were extracted from the ROI and converted to contrast concentration values (Fig. 6). In two patients, contrast inflow was observed directly at the start of the image series. In one patient, the fitting was unsuccessful. For these cases, population-based median AIF and VIF values were computed from the mean values of the individual curves (Appendix C). Subsequently, pharmacokinetic modeling using Sourbron's model was applied to all images. DCE-MRI parameters (F_a, F_v and K_i) were computed for the entire liver, FLR and ROIs in the FLR (Table 2 and 3). Besides the values derived from the parametric maps, the total in-flow ($T_f = F_a + F_v$) and arterial plasma flow fraction ($f_a = (F_a/F_a + F_v)$) were computed.

Table 1: Patient Characteristics

Age (mean)	63 years
Sex female/male	8/11
Type of Liver Disease	
HCC	3/19
Benign	4/19
CRLM	8/19
PHC	1/19
IHC	3/19
Resection left/right	15/4
METAVIR	
F0	12/19
F1	4/19
F2	2/19
F3	0/19
F4	1/19

Hepatocellular Carcinoma (HCC), Colorectal Liver Metastases (CRLM), Perihilar Cholangiocarcinoma (PHC), Intrahepatic Cholangiocarcinoma (IHC)
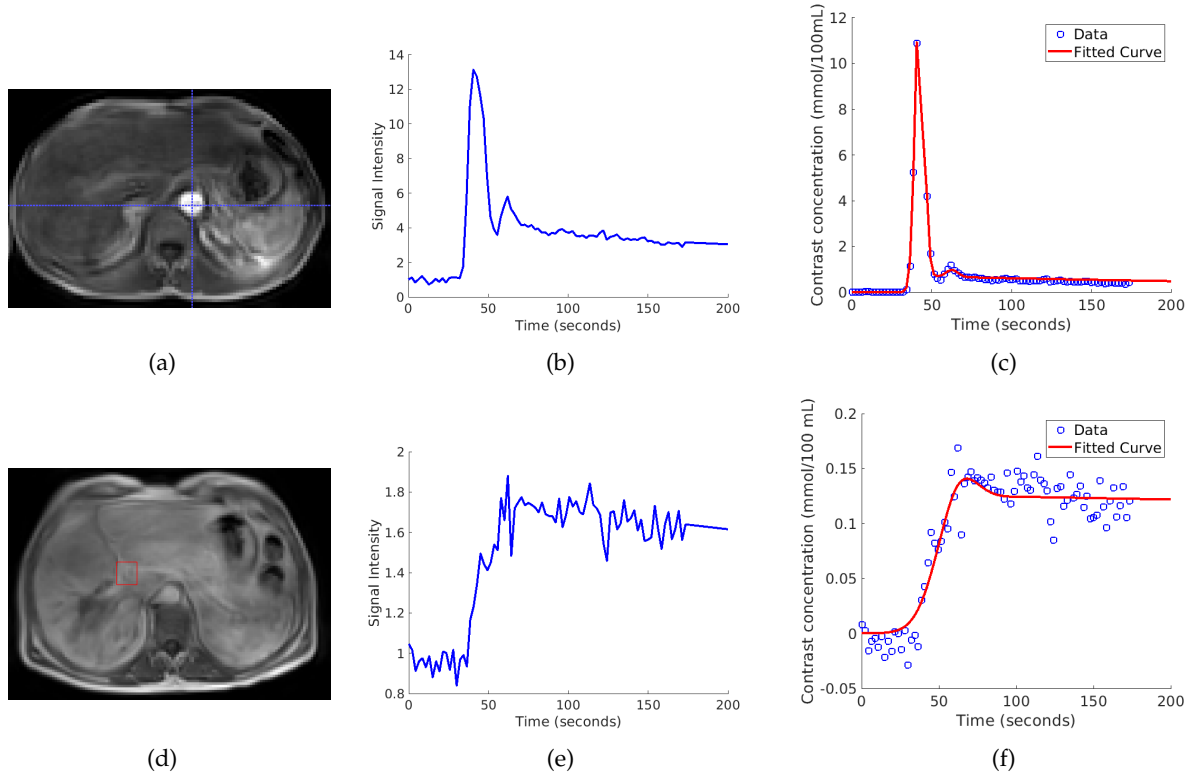
Figure 6: Computation of AIF and VIF. Image (a) and (d) display axial magnetic resonance imaging slices highlighting regions of interest for arterial and venous inputs. Graph (b) and (e) depict the derived TICs from these regions. Graph (c) and (f) display the analytical fits for AIF and VIF, respectively.

Table 2: Descriptive Statistics for TLF and FLR Values

	Parameter	N	Minimum	Maximum	Mean	SD
HBS	MUR TLV	19	7,50	20,47	15,22	3,41
	MUR FLR	19	2,10	12,60	4,89	2,84
DCE	K_i TLV	19	2,69	11,45	6,91	2,93
	K_i FLR	19	2,44	12,28	7,09	1,65
	F_a TLV	19	6,46	52,77	22,90	15,46
	F_a FLR	19	5,11	53,32	20,97	14,64
	F_v TLV	19	7,42	67,55	30,73	18,67
	F_v FLR	19	7,28	91,94	31,91	23,17

MUR, mebrofenin uptake rate (%/min); K_i, Primovist uptake rate (min^{-1}); TLV, Total Liver Volume; FLR, Future Liver Remnant.

4.2.3 IVIM

The methodology was successfully applied to process the IVIM images (Appendix B). However, parameter extraction from the entire liver, FLR segmentation, and several Couinaud segments was not feasible due to these segments being outside the field of view. Consequently, IVIM-MRI parameters ((D, D_p, and f) were extracted from the available ROIs. The mean values of IVIM-MRI ROI measurements within the FLR are displayed in Table 3.

Table 3: Descriptive Statistics for ROI Values in the FLR

	Parameter	N	Minimum	Maximum	Mean	SD
DCE	K_i	19	2.44	19.22	8.47	3.92
	F_a	19	2.60	53.26	21.65	16.34
	F_p	19	2.40	93.33	36.42	30.39
IVIM	D	19	0.67	2.34	1.60	0.40
	D_p	19	39.43	122.73	85.30	22.59
	P_F	19	4.24	24.92	13.65	6.61

K_i, Primovist uptake rate (min^{-1}); D, diffusion coefficient ($10^{-3}\ \text{mm}^2/\text{s}$); D_p, pseudodiffusion coefficient ($10^{-3}\ \text{mm}^2/\text{s}$); f, perfusion fraction (%); F_a, arterial plasma flow (mL/min/100mL); F_p, venous plasma flow (mL/min/100mL);

4.3 Statistical analysis

4.3.1 Correlation of DCE-MRI and HBS parameters

A Bland-Altman analysis was conducted to assess the agreement between the functional share values from HBS and DCE-MRI. The analysis revealed a mean difference of 0.52 with limits of agreement ranging from -15.21 to 16.24, indicating a generally strong agreement with some variability between the measurements. A Pearson correlation analysis was conducted to assess the relationship between the TLF function and FLR function from both DCE-MRI and HBS. Additionally, a sub-analysis was conducted for patients who underwent right hepatectomy. The correlation between the DCE-MRI parameter K_i and the HBS parameter MUR showed a moderate positive correlation (r = 0.49, p = 0.03) (Fig. 7a). Additionally, there was a strong, significant correlation between the FLR MUR and K_i (r = 0.80, p <0.001) (Fig. 7b) in the whole patient group. Whereas a weak correlation was observed between the FLR MUR and K_i in the right hepatectomy group (r = 0.214, p = 0.443) (Fig. 7c).

(a)   (b)   (c)
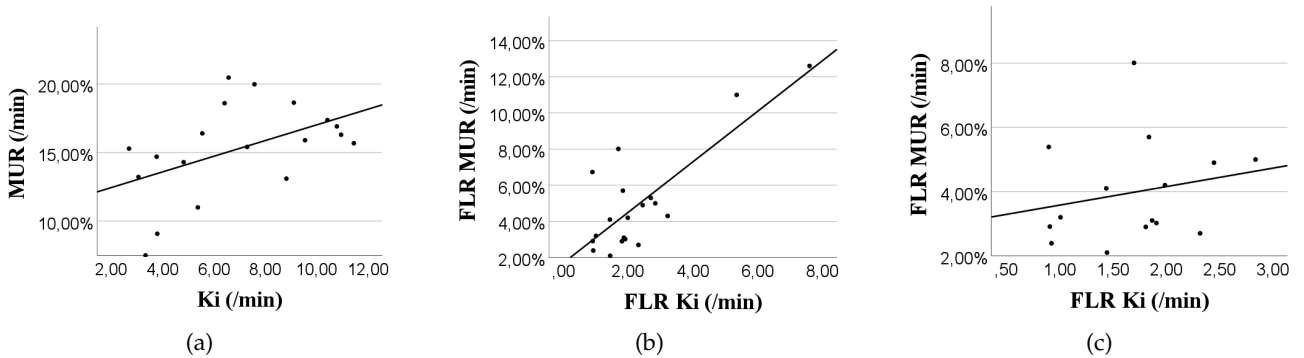
Figure 7: Pearson correlation between total liver function, as measured with HBS and DCE. Results are demonstrated for the total liver (a), the future liver remnant of all patients (b) and the future liver remnant in patients who underwent right hepatectomy (c). FLR, Future Liver Remanant; K_i, Primovist uptake rate (min^{-1}); MUR, Mebrofenin uptake rate (min^{-1}).

4.3.2 Interobserver variability DCE-MRI

The Bland-Altman analysis was employed to assess the reproducibility of the DCE-MRI measurements. The results demonstrated a mean bias of -0.08 for functional share, with limits of agreement from -1.98 to 1.82, indicating strong reproducibility. FLR Function had a mean bias of -0.12 and limits from -4.85 to 4.60. TLF demonstrated more variability, with a mean bias of -1.79 and limits from -20.07 to 16.49.

4.3.3 Correlation of DCE- and IVIM-MRI parameters

Table 4 presents the Pearson correlations between the DCE-MRI parameters (K_i, F_v, F_a, T_f and f_a) and the IVIM-MRI parameters (D, D_p, and f). This analysis demonstrated negative weak to positive moderate correlations ($r = -0.326$ to $r = 0.443$).

Table 4: Pearson correlations between DCE parameters and IVIM parameters

DCE		IVIM		
		D	D_p	f
K_i	r	0.149	-0.143	0.059
	p	0.542	0.560	0.811
F_a	r	0.443	-0.326	-0.064
	p	0.057	0.173	0.793
F_v	r	0.074	0.144	-0.169
	p	0.763	0.555	0.489
T_f	r	0.300	-0.030	-0.196
	p	0.211	0.904	0.422
f_a	r	0.055	-0.200	0.130
	p	0.823	0.411	0.597

The significance level was set at $p < 0.05$. K_i, Primovist uptake rate (min^{-1}); F_a, arterial plasma flow (mL/min/100mL); F_v, venous plasma flow (mL/min/100mL); T_f, total plasma flow (mL/min/100mL); f_a, arterial plasma flow fraction (%). D_p, pseudodiffusion coefficient (10^{-3} mm^2/s); D, diffusion coefficient (10^{-3} mm^2/s); f, perfusion fraction (%).

4.3.4 Correlation of IVIM-MRI and histological parameters

Correlation between IVI-MRI parameters and the histological METAVIR score was examined. The correlation coefficients were as follows: D (r = 0.374, p = 0.115), D_p (r = -0.199, p = 0.415), and f (r = -0.252, p = 0.298). These results suggest a weak correlation between the IVIM-MRI parameters and METAVIR scores.

Discussion

The aim of this study was to examine the relationship between IVIM- and DCE-MRI in the assessment of preoperative liver function in patients scheduled for major hepatectomy. The results indicated a negative weak to positive moderate correlation between IVIM- and DCE-MRI parameters. Additionally, strong correlations were observed between the hepatic uptake rate K_i measured by DCE-MRI and the MUR measured by HBS. High reproducibility with minimal bias was also observed in the repeated DCE-MRI analysis.

The lack of correlation between DCE- and IVIM-MRI parameters may be attributed to the fundamental differences in measurement techniques and the physiological processes they detect. DCE-MRI quantifies liver-specific contrast uptake, determined by multiple physiological factors, including perfusion, permeability, diffusion, and active hepatocyte transport. In contrast, IVIM-MRI measures diffusion and perfusion without the use of contrast agents. Previous studies have demonstrated that IVIM-MRI has good diagnostic accuracy in detecting and staging liver fibrosis. However, the limited representation of advanced fibrosis stages in our patient cohort may have contributed to the lack of correlations observed with histological parameters. This may also explain the discrepancies between our findings and those of Hectors and Phonlakrai et al., who assessed the correlation between IVIM- and DCE-MRI in a cohort of patients with HCC[22]. Unlike our cohort, which almost exclusively included patients undergoing major liver resections without evident liver pathology, patients with HCC often present with fibrosis or cirrhosis[23]. These underlying conditions may contribute to the moderate correlations (f_a and D_p ($r = -0.443$, $P = 0.028$); f_a and f ($r = -0.536$, $P = 0.006$); F_a and f ($r = -0.455$, $P = 0.023$)) observed in their findings. This is supported by studies demonstrating a correlation

between IVIM-MRI measurements and the Child-Pugh scoring system, which is employed to assess the severity of cirrhosis[36].

IVIM-MRI values reported in the literature vary widely due to differences in imaging protocols, MRI systems, and analysis methods[21]. Nevertheless, our IVIM-MRI results align with previously reported values, which range from 0.66–1.50 for D (10^{-3} mm^2/s), 13.60–136 (10^{-3} mm^2/s) for D_p, and 5.50–47.7% for f[21, 37, 38]. The mean D in our study (1.60) was slightly higher compared to other studies, which may have attributed to the limited range of b-values used (0 to 294 mm²/s). These b-values primarily capture perfusion effects rather than pure diffusion, potentially reducing sensitivity to slow diffusion components and affecting the accuracy of D measurements. This limitation might also explain the correlations observed between D and K_i measured with DCE-MRI. In contrast, previous research by Hectors et al. employed a broader range of b-values, allowing for a more accurate separation of diffusion from perfusion effects[23]. This wider range likely enhanced the quantification of diffusion and may account for the moderate correlations observed in their study.

The low bias observed in the Bland-Altman tests indicates high consistency and reliability across the repeated DCE-MRI post-processing analysis, despite the variability introduced by manual processing steps. The variability may be attributed to different registration methods employed compared to the previous study[18]. In addition, in our study, population-based parameters for VIF and AIF were applied in three patients. However, this may not accurately reflect the individual input function, leading to significant errors in the computation of pharmacokinetic parameters[39]. The slightly weaker correlation observed in DCE-MRI measurements in our analysis ($r = 0.80$, $p < 0.001$) compared to the correlations reported by Rassam et al. ($r = 0.89$, $p < 0.001$) may be a result of the observed variability[18].

Moderate correlations were observed in the whole liver, while strong correlations were found in the FLR. However, in the patients that underwent right hepatectomy, the correlation between FLR MUR and K_i was weak ($r = 0.214$, $p = 0.443$). This indicates that the relationship between the FLR MUR and K_i is less evident in the left liver lobes. The correlation observed between the FLR in all patients may be based on the functional dominance of the right liver lobe segments, rather than indicating a direct relationship between DCE-MRI and HBS[40].

The strong correlation observed between DCE-MRI and HBS indicates that DCE-MRI may serve as an alternative for evaluating preoperative liver function. This could create a "one-stop shop" MRI for preoperative planning, allowing for simultaneous assessment of liver function, anatomy, and tumor characterization. However, future studies are needed to address the challenges of clinical implementation, which is currently unfeasible due to complex pharmacokinetic models, variability in post-processing measurements, and a lack of standardization. While IVIM-MRI did not demonstrate strong correlations with DCE-MRI parameters in this specific patient cohort, it may still provide valuable complementary information for preoperative planning. For instance, the diagnostic performance of IVIM-MRI for detecting liver fibrosis demonstrated high accuracy across fibrosis stages, with AUCs of 0.862 (95% CI: 0.811–0.914) for $\geq F1$, 0.883 (95% CI: 0.856–0.909) for $\geq F2$, 0.886 (95% CI: 0.865–0.907) for $\geq F3$, and 0.899 (95% CI: 0.866–0.932) for $F4$[41]. Moreover, compared to the conventional tumor characterization with DWI-MRI to distinguish benign from malignant lesions and primary from secondary tumors[42].

In addition to the investigated MRI techniques in our study, other quantitative MRI techniques have been developed to evaluate liver characteristics. For instance, fat fractions and stiffness quantification through proton density fat fraction MRI and magnetic resonance elastography MRI are already employed in clinical practice[43, 44]. Additionally, there is no evidence demonstrating a direct correlation between individual liver pathology measurements and liver function[11]. However, it is possible that the collective effects of different types of liver pathology influence overall liver functionality in varying ways. Integrating various MRI techniques into a multiparametric approach could significantly enhance our understanding of liver disease and its relation to liver function and regenerative capacity. LiverMultiScan has developed a tool that quantifies liver steatosis, fibrosis, and iron overload using multiparametric MRI[45, 46]. The impact of underlying liver disease on the risk of PHLF requires careful consideration. Distinguishing borderline resectable patients presents a challenge due to the resilience of the liver, which often obscures underlying pathology in individuals with compromised liver

function.

This study has several limitations that should be considered when interpreting the results. First, the manual delineation of the portal vein, future remnant liver, and ROIs may have introduced observer bias. Manual processing can lead to variability in results, affecting the reliability of the findings, especially when performed by an inexperienced or non-clinician. Additionally, due to the incomplete coverage of the liver in the field of view in the scan, whole liver or segmental liver delineation on IVIM images was impossible. As a result, ROIs only capture a small portion of the liver, which may not represent the heterogeneity of the whole liver or individual segments. This limitation can lead to a biased or incomplete assessment of liver conditions.

Another limitation was the change in the imaging protocol during the study, which resulted in variations in the volumes and timing of contrast inflow. This made post-processing more complex and could have affected the consistency of the data. Furthermore, our patient group was relatively homogeneous, primarily consisting of patients with CRLM, who generally have adequate liver function. This homogeneity may impact the observed correlations due to the lack of variability in liver function within our patient group. Finally, T1-relaxometry values from the literature were employed instead of patient-specific T1 maps, which could have impacted the accuracy of the imaging analyses.

These limitations highlight the need for further studies with larger and more diverse patient populations, as well as standardized imaging protocols, to validate our findings. Future research should explore these imaging modalities in different liver diseases and heterogeneous liver function cohorts. Standardization of image acquisition and post-processing techniques is crucial for enhancing the reliability and comparability of liver imaging studies. For instance, the incorporation of automated liver segmentation algorithms will improve reproducibility and consistency in post-processing compared to manual segmentation methods. Moreover, other potential sources of bias, such as variability across scanners and inter-time variability, should be considered to ensure the reproducibility and accuracy of the results.

Conclusion

The lack of correlation between DCE and IVIM-MRI parameters indicates the limited utility of IVIM-MRI in preoperative liver function evaluation. The strong correlations observed between DCE-MRI and HBS parameters suggest that DCE-MRI may serve as a viable alternative for assessing liver function in preoperative settings. However, further studies in a patient cohort with varying degrees of liver function are essential to validate the observed correlations and assess the clinical applicability of IVIM- and DCE-MRI.

References

[1] E. Trefts, M. Gannon, and D. H. Wasserman. "The liver". In: *Current Biology* 27.21 (2017). Accession Number: 29112863, PMCID: PMC5897118, R1147–R1151. DOI: 10.1016/j.cub.2017.09.019. URL: https://www.ncbi.nlm.nih.gov/pubmed/29112863.

[2] G. K. Michalopoulos and B. Bhushan. "Liver regeneration: biological and pathological mechanisms and implications". In: *Nature Reviews Gastroenterology and Hepatology* 18.1 (2021). Accession Number: 32764740, pp. 40–55. DOI: 10.1038/s41575-020-0342-4. URL: https://www.ncbi.nlm.nih.gov/pubmed/32764740.

[3] A. Elgendy. *Couinaud classification (diagram)*. Case study, Radiopaedia.org. Accessed on 02 Jul 2024. 2024. URL: https://doi.org/10.53347/rID-63998.

[4] A. Sharma and S. Nagalli. "Chronic Liver Disease". In: *StatPearls [Internet]*. Updated 2023 Jul 3. Treasure Island (FL): StatPearls Publishing, 2024. URL: https://www.ncbi.nlm.nih.gov/books/NBK554597/.

[5] J. M. Llovet et al. "Hepatocellular carcinoma". In: *Nature Reviews Disease Primers* 7.1 (2021). Accession Number: 33479224, p. 6. DOI: 10.1038/s41572-020-00240-3. URL: https://www.ncbi.nlm.nih.gov/pubmed/33479224.

[6] S. Bangru and A. Kalsotra. "Cellular and molecular basis of liver regeneration". In: *Seminars in Cell and Developmental Biology* 100 (2020). Accession Number: 31980376, PMCID: PMC7108750, pp. 74–87. DOI: 10.1016/j.semcdb.2019.12.004. URL: https://www.ncbi.nlm.nih.gov/pubmed/31980376.

[7] E. Zuniga-Aguilar and O. Ramirez-Fernandez. "Fibrosis and hepatic regeneration mechanism". In: *Transl Gastroenterol Hepatol* 7 (2022), p. 9. DOI: 10.21037/tgh.2020.02.21.

[8] A. Ananthakrishnan, V. Gogineni, and K. Saeian. "Epidemiology of primary and secondary liver cancers". In: *Semin Intervent Radiol* 23.1 (2006), pp. 47–63. DOI: 10.1055/s-2006-939841. URL: https://www.ncbi.nlm.nih.gov/pubmed/21326720.

[9] A. M. van Keulen et al. "Primary and secondary liver failure after major liver resection for perihilar cholangiocarcinoma". In: *Surgery* 170.4 (2021), pp. 1024–1030. DOI: 10.1016/j.surg.2021.04.013.

[10] A. Guglielmi et al. "How much remnant is enough in liver resection?" In: *Digestive Surgery* 29.1 (2012), pp. 6–17. DOI: 10.1159/000335713. URL: https://www.ncbi.nlm.nih.gov/pubmed/22441614.

[11] F. Primavesi et al. "E-AHPBA-ESSO-ESSR Innsbruck consensus guidelines for preoperative liver function assessment before hepatectomy". In: *Br J Surg* 110.10 (2023), pp. 1331–1347. DOI: 10.1093/bjs/znad233.

[12] P. Arntz and P. B. Olthof. "Assessment of liver function before major hepatectomy". In: *Br J Surg* 110.12 (2023), pp. 1588–1589. DOI: 10.1093/bjs/znad216. URL: https://www.ncbi.nlm.nih.gov/pubmed/37531456.

[13] P. B. Olthof et al. "Hepatobiliary scintigraphy to predict postoperative liver failure after major liver resection; a multicenter cohort study in 547 patients". In: *HPB (Oxford)* 25.4 (2023), pp. 417–424. DOI: 10.1016/j.hpb.2022.12.005. URL: https://www.ncbi.nlm.nih.gov/pubmed/36759303.

[14] R. A. Novelline. *Squire's Fundamentals of Radiology*. 6th. Cambridge, MA: Harvard University Press, 2004.

[15] D. Le Bihan and R. Turner. "The capillary network: a link between IVIM and classical perfusion". In: *Magnetic Resonance in Medicine* 27.1 (1992). Accession Number: 1435202, pp. 171–178. DOI: 10.1002/mrm.1910270116. URL: https://www.ncbi.nlm.nih.gov/pubmed/1435202.

[16] C. Rio Bartulos et al. "Assessment of Liver Function With MRI: Where Do We Stand?" In: *Front Med (Lausanne)* 9 (2022), p. 839919. DOI: 10.3389/fmed.2022.839919.

[17] R. K. Do, H. Rusinek, and B. Taouli. "Dynamic contrast-enhanced MR imaging of the liver: current status and future directions". In: *Magnetic Resonance Imaging Clinics of North America* 17.2 (2009). Accession Number: 19406362, pp. 339–349. DOI: 10.1016/j.mric.2009.01.009. URL: https://www.ncbi.nlm.nih.gov/pubmed/19406362.

[18] F. Rassam et al. "Comparison between dynamic gadoxetate-enhanced MRI and (99m)Tc-mebrofenin hepatobiliary scintigraphy with SPECT for quantitative assessment of liver function". In: *Eur Radiol* 29.9 (2019), pp. 5063–5072. DOI: 10.1007/s00330-019-06029-7.

[19] Y. Cao et al. "Prediction of liver function by using magnetic resonance-based portal venous perfusion imaging". In: *Int J Radiat Oncol Biol Phys* 85.1 (2013), pp. 258–263. DOI: 10.1016/j.ijrobp.2012.02.037.

[20] J. Simeth et al. "Quantification of liver function by linearization of a two-compartment model of gadoxetic acid uptake using dynamic contrast-enhanced magnetic resonance imaging". In: *NMR Biomed* 31.6 (2018), e3913. DOI: 10.1002/nbm.3913.

[21] Y. T. Li et al. "Liver intravoxel incoherent motion (IVIM) magnetic resonance imaging: a comprehensive review of published data on normal values and applications for fibrosis and tumor evaluation". In: *Quant Imaging Med Surg* 7.1 (2017), pp. 59–78. DOI: 10.21037/qims.2017.02.03.

[22] M. Phonlakrai et al. "Non-contrast based approach for liver function quantification using Bayesian-based intravoxel incoherent motion diffusion weighted imaging: A pilot study". In: *J Appl Clin Med Phys* 24.11 (2023), e14178. DOI: 10.1002/acm2.14178.

[23] S. J. Hectors et al. "Intravoxel incoherent motion diffusion-weighted imaging of hepatocellular carcinoma: Is there a correlation with flow and perfusion metrics obtained with dynamic contrast-enhanced MRI?" In: *J Magn Reson Imaging* 44.4 (2016), pp. 856–864. DOI: 10.1002/jmri.25194.

[24] P. J. W. Arntz et al. "Joint EANM/SNMMI/IHPBA procedure guideline for [(99m)Tc]Tc-mebrofenin hepatobiliary scintigraphy SPECT/CT in the quantitative assessment of the future liver remnant function". In: *HPB (Oxford)* 25.10 (2023), pp. 1131–1144. DOI: 10.1016/j.hpb.2023.06.001.

[25] M. Ekman et al. "Liver uptake function measured by IODIDA clearance rate in liver transplant patients and healthy volunteers". In: *Nuclear Medicine Communications* 17.3 (1996), pp. 235–242. DOI: 10.1097/00006231-199603000-00011.

[26] M. R. Orton et al. "Computationally efficient vascular input function models for quantitative kinetic modelling using DCE-MRI". In: *Physics in Medicine and Biology* 53.5 (2008), pp. 1225–1239. ISSN: 0031-9155. DOI: 10.1088/0031-9155/53/5/005.

[27] S. Sourbron et al. "Combined quantification of liver perfusion and function with dynamic gadoxetic acid-enhanced MR imaging". In: *Radiology* 263.3 (2012), pp. 874–883. ISSN: 0033-8419. DOI: 10.1148/radiol.12110337.

[28] M. Rohrer et al. "Comparison of magnetic properties of MRI contrast media solutions at different magnetic field strengths". In: *Investigative Radiology* 40.11 (2005), pp. 715–724. ISSN: 0020-9996. DOI: 10.1097/01.rli.0000184756.66360.d3.

[29] H. Lu et al. "Determining the longitudinal relaxation time (T1) of blood at 3.0 Tesla". In: *Magnetic Resonance in Medicine* 52.3 (2004), pp. 679–682. ISSN: 0740-3194. DOI: 10.1002/mrm.20178.

[30] T. Zhang et al. "A pharmacokinetic model including arrival time for two inputs and compensating for varying applied flip-angle in dynamic gadoxetic acid-enhanced MR imaging". In: *PLoS One* 14.8 (2019), e0220835. ISSN: 1932-6203. DOI: 10.1371/journal.pone.0220835.

[31] C. Eipel, K. Abshagen, and B. Vollmar. "Regulation of hepatic blood flow: the hepatic arterial buffer response revisited". In: *World Journal of Gastroenterology* 16.48 (2010). Accession Number: 21182219, PMCID: PMC3012579, pp. 6046–6057. DOI: 10.3748/wjg.v16.i48.6046. URL: https://www.ncbi.nlm.nih.gov/pubmed/21182219.

[32] P. A. Yushkevich, G. Yang, and G. Gerig. "ITK-SNAP: An interactive tool for semi-automatic segmentation of multi-modality biomedical images". In: *Annual International Conference of the IEEE Engineering in Medicine and Biology Society (EMBC)*. Accession Number: 28269019, PMCID: PMC5493443. 2016, pp. 3342–3345. DOI: 10.1109/EMBC.2016.7591443. URL: https://www.ncbi.nlm.nih.gov/pubmed/28269019.

[33] S. Barbieri et al. "Deep learning how to fit an intravoxel incoherent motion model to diffusion-weighted MRI". In: *Magnetic Resonance in Medicine* 83.1 (2020). Accession Number: 31389081, pp. 312–321. DOI: 10.1002/mrm.27910. URL: https://www.ncbi.nlm.nih.gov/pubmed/31389081.

[34] M. P. T. Kaandorp et al. "Deep learning intravoxel incoherent motion modeling: Exploring the impact of training features and learning strategies". In: *Magnetic Resonance in Medicine* 90.1 (2023). Accession Number: 36912473, pp. 312–328. DOI: 10.1002/mrm.29628. URL: https://www.ncbi.nlm.nih.gov/pubmed/36912473.

[35] C. A. Campo et al. "Standardized Approach for ROI-Based Measurements of Proton Density Fat Fraction and R2* in the Liver". In: *AJR Am J Roentgenol* 209.3 (2017), pp. 592–603. DOI: 10.2214/AJR.17.17812.

[36] L. Ding et al. "Intravoxel Incoherent Motion (IVIM) Diffusion-Weighted Imaging (DWI) in Patients with Liver Dysfunction of Chronic Viral Hepatitis: Segmental Heterogeneity and Relationship with Child-Turcotte-Pugh Class at 3 Tesla". In: *Gastroenterology Research and Practice* 2018 (2018). Accession Number: 30647733, PMCID: PMC6311737, p. 2983725. DOI: 10.1155/2018/2983725. URL: https://www.ncbi.nlm.nih.gov/pubmed/30647733.

[37] Y. Shan et al. "Comparison of Free-Breathing With Navigator-Triggered Technique in Diffusion Weighted Imaging for Evaluation of Small Hepatocellular Carcinoma: Effect on Image Quality and Intravoxel Incoherent Motion Parameters". In: *Journal of Computer Assisted Tomography* 39.5 (2015). Accession Number: 26196345, pp. 709–715. DOI: `10.1097/RCT.0000000000000278`. URL: `https://www.ncbi.nlm.nih.gov/pubmed/26196345`.

[38] H. Watanabe et al. "Characterizing focal hepatic lesions by free-breathing intravoxel incoherent motion MRI at 3.0 T". In: *Acta Radiologica* 55.10 (2014). Accession Number: 24316660, pp. 1166–1173. DOI: `10.1177/0284185113514966`. URL: `https://www.ncbi.nlm.nih.gov/pubmed/24316660`.

[39] H. L. Cheng. "Investigation and optimization of parameter accuracy in dynamic contrast-enhanced MRI". In: *Journal of Magnetic Resonance Imaging* 28.3 (2008). Accession Number: 18777534, pp. 736–743. DOI: `10.1002/jmri.21489`. URL: `https://www.ncbi.nlm.nih.gov/pubmed/18777534`.

[40] H. Nilsson et al. "The inhomogeneous distribution of liver function: possible impact on the prediction of post-operative remnant liver function". In: *HPB (Oxford)* 17.3 (2015). Accession Number: 25297934, PMCID: PMC4333790, pp. 272–277. DOI: `10.1111/hpb.12348`. URL: `https://www.ncbi.nlm.nih.gov/pubmed/25297934`.

[41] Z. Ye et al. "Value of intravoxel incoherent motion in detecting and staging liver fibrosis: A meta-analysis". In: *World J Gastroenterol* 26.23 (2020), pp. 3304–3317. DOI: `10.3748/wjg.v26.i23.3304`.

[42] J. H. Yoon et al. "Evaluation of hepatic focal lesions using diffusion-weighted MR imaging: comparison of apparent diffusion coefficient and intravoxel incoherent motion-derived parameters". In: *Journal of Magnetic Resonance Imaging* 39.2 (2014). Accession Number: 23633178, pp. 276–285. DOI: `10.1002/jmri.24158`. URL: `https://www.ncbi.nlm.nih.gov/pubmed/23633178`.

[43] J. Bi, L. Liu, and T. Qin. "Comparison of magnetic resonance elastography and transient elastography in the diagnosis of hepatic fibrosis: a systematic review and meta-analysis". In: *Annals of Palliative Medicine* 10.8 (2021). Accession Number: 34488358, pp. 8692–8700. DOI: `10.21037/apm-21-1176`. URL: `https://www.ncbi.nlm.nih.gov/pubmed/34488358`.

[44] J. Gu et al. "Diagnostic value of MRI-PDFF for hepatic steatosis in patients with non-alcoholic fatty liver disease: a meta-analysis". In: *European Radiology* 29.7 (2019). Accession Number: 30899974, pp. 3564–3573. DOI: `10.1007/s00330-019-06072-4`. URL: `https://www.ncbi.nlm.nih.gov/pubmed/30899974`.

[45] D. J. Mole et al. "Study protocol: HepaT1ca - an observational clinical cohort study to quantify liver health in surgical candidates for liver malignancies". In: *BMC Cancer* 18.1 (2018). Accession Number: 30208871, PMCID: PMC6136162, p. 890. DOI: `10.1186/s12885-018-4737-3`. URL: `https://www.ncbi.nlm.nih.gov/pubmed/30208871`.

[46] N. McDonald et al. "Multiparametric magnetic resonance imaging for quantitation of liver disease: a two-centre cross-sectional observational study". In: *Scientific Reports* 8.1 (2018). Accession Number: 29907829, PMCID: PMC6003924, p. 9189. DOI: `10.1038/s41598-018-27560-5`. URL: `https://www.ncbi.nlm.nih.gov/pubmed/29907829`.

Appendix A

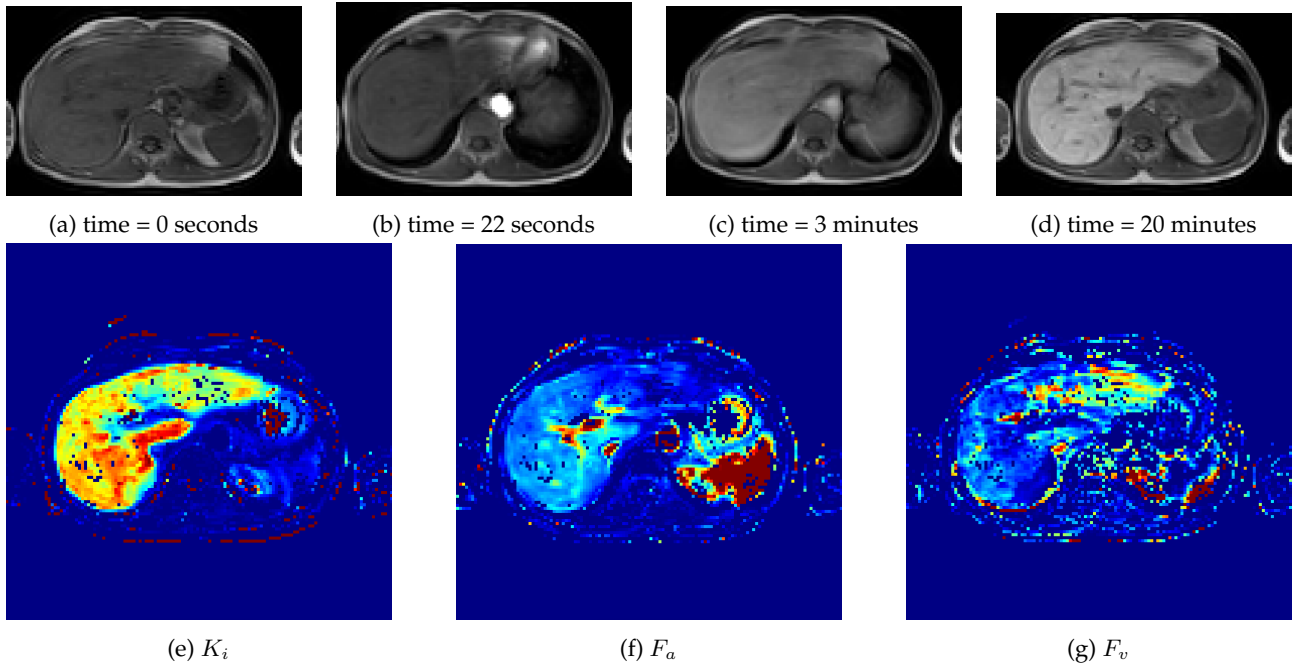| (a) time = 0 seconds | (b) time = 22 seconds | (c) time = 3 minutes | (d) time = 20 minutes |

(e) K_i (f) F_a (g) F_v

Figure A.1: DCE MRI images at various stages: (a) initial image at time 0, (b) arterial phase post-contrast injection, (c) portal venous phase, (d) hepatobiliary phase at 20 minutes, (e) hepatic uptake rate map K_i (min^{-1}), (f) arterial plasma flow F_a map (mL/min/100mL), and (g) venous plasma flow F_v map (mL/min/100mL).

Appendix B

(a) b = 0

(b) b = 1

(c) b = 2

(d) b = 4

(e) b = 6

(f) b = 9

(g) b = 12

(h) b = 17

(i) b = 24

(j) b = 37

(k) b = 54

(l) b = 98

(m) b = 147
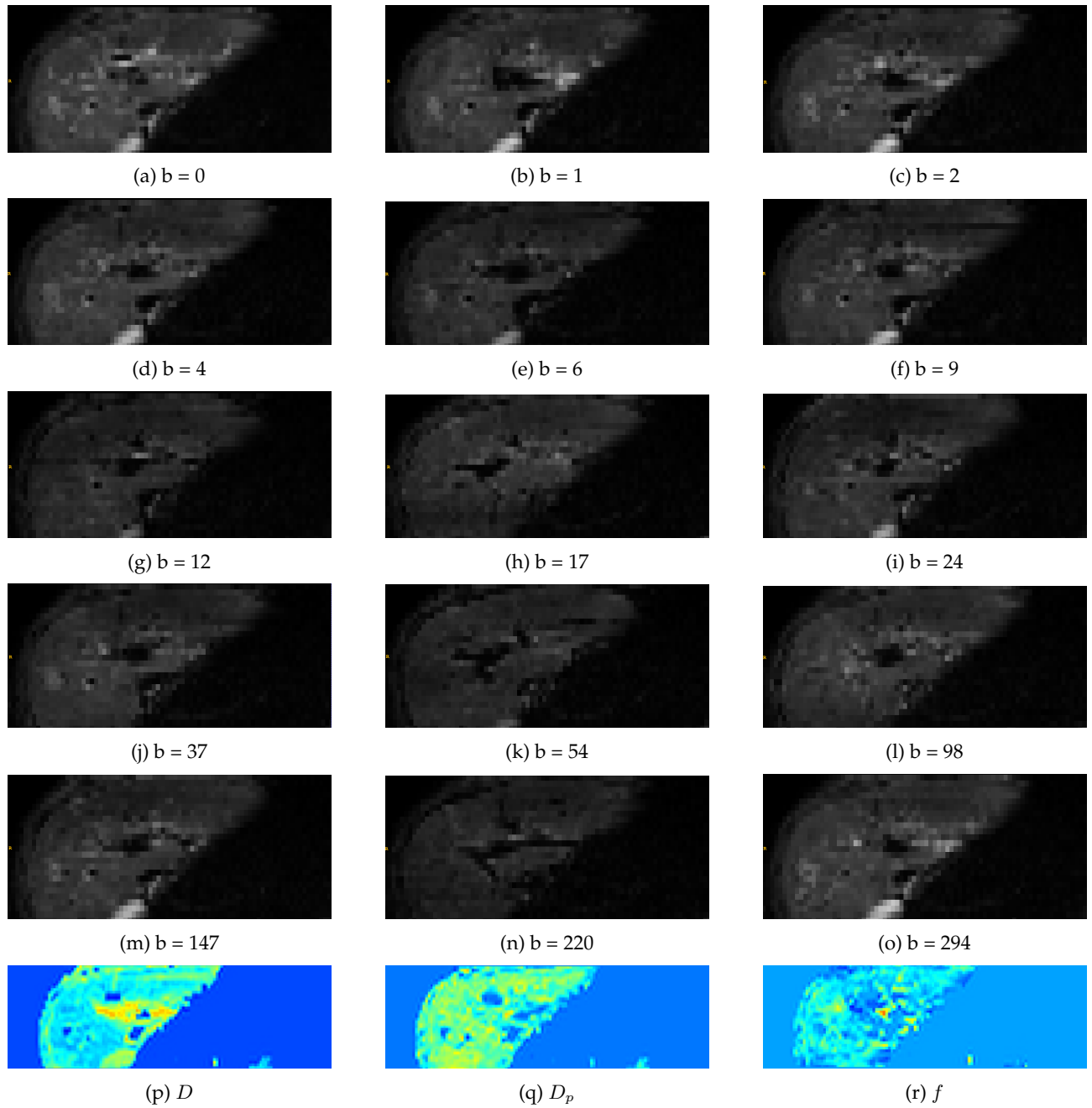
(n) b = 220

(o) b = 294

(p) D

(q) D_p

(r) f

Figure B.1: (a-o) Diffusion weighted images with different b-values. Each subfigure corresponds to a specific b-value. (p-q) Reoriented parametric maps after IVIM image processing. D, diffusion (mm^2/s); D_p, pseudodiffusion (mm^2/s); f, perfusion fraction (%).

Appendix C

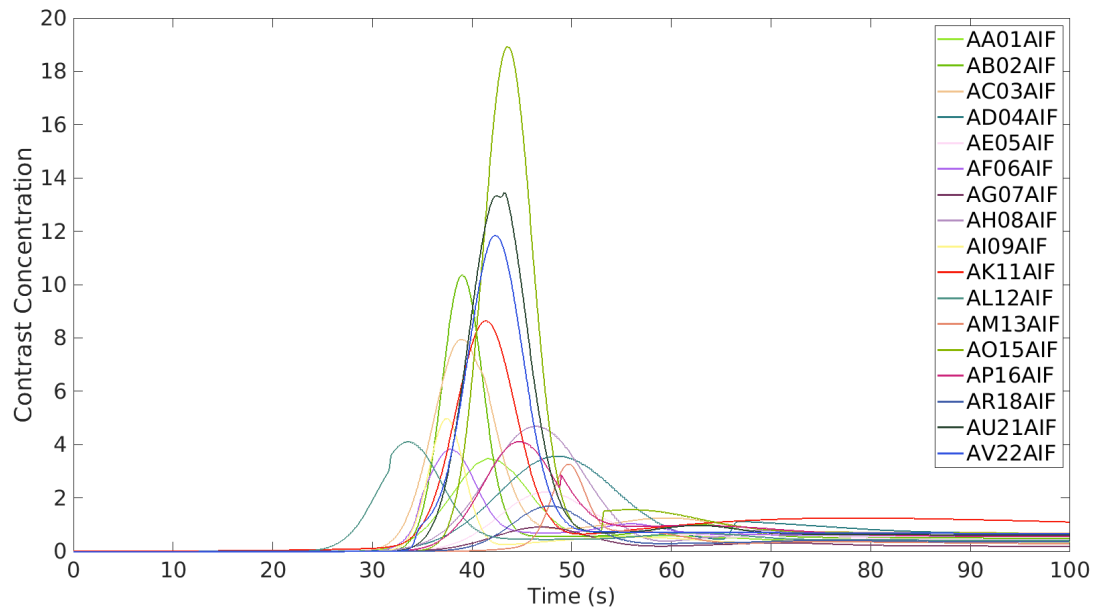## C.1 Individual AIF and VIF curves

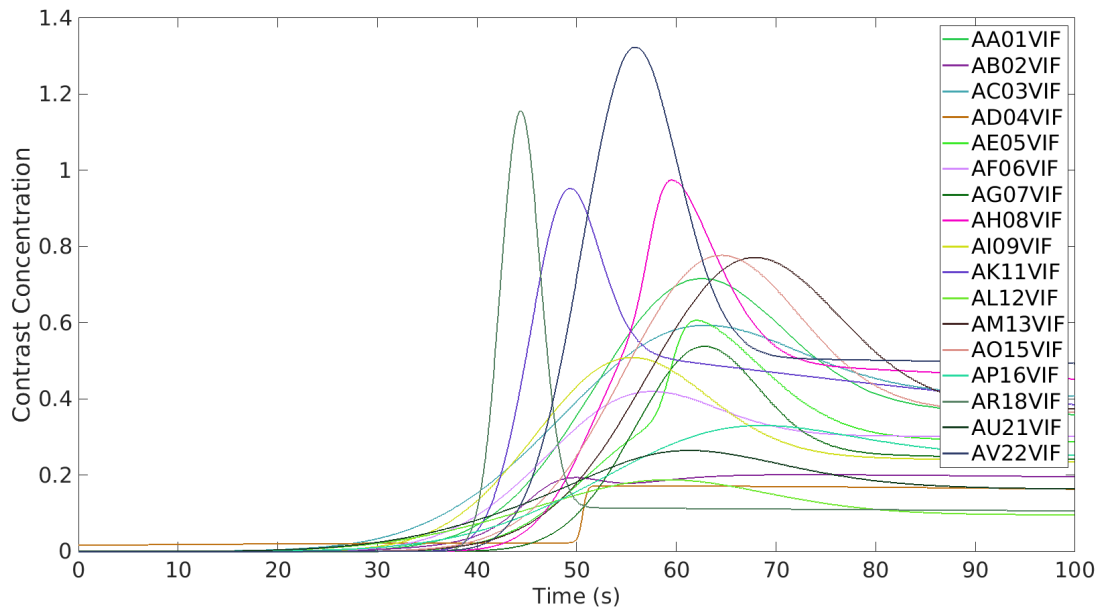Figure C.1: Individual arterial input functions

Figure C.2: Individual venous input functions
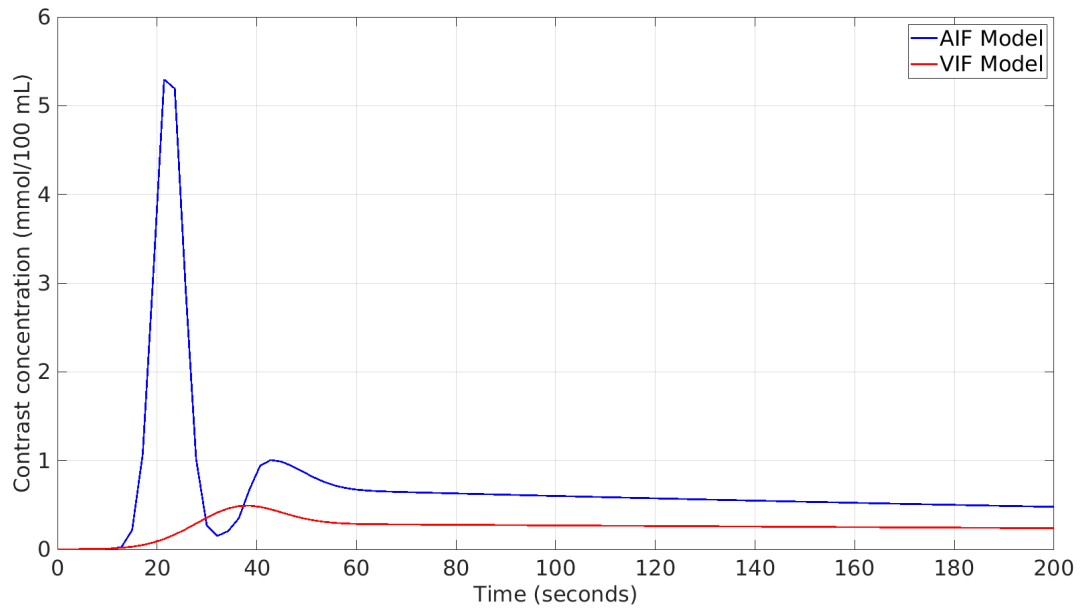
C.2 population based AIF and VIF curves

Figure C.3: Population based arterial and venous input function

Appendix D

Quantitative MRI in the pre-operative evaluation of liver function for hepatectomy – a scoping review

Fenna A. van der Zijden [a,b], Pieter J.W. Arntz [b,c]

[a] *MSc Student Technical Medicine, Technical University Delft, Leiden University Medical Center, Erasmus Medical Center, The Netherlands* [b] *Cancer Center Amsterdam, The Netherlands* [c] *Department of Surgery, Amsterdam UMC, University of Amsterdam, The Netherlands*

Abstract

Background: Careful assessment of remnant liver function before liver resection is essential to minimize the risk of post-hepatectomy liver failure (PHLF). Quantitative magnetic resonance imaging (qMRI) has emerged as potential technique for evaluating liver function, predicting PHLF, and assessing underlying liver diseases. However, the application of qMRI in the preoperative evaluation for liver surgery is limited. The aim of this review is to present an overview of the role of qMRI in the preoperative assessment for liver surgery. Methods: A systematic review was conducted for qMRI sequences compared to preoperative tests to measure liver function as mentioned in the E-AHPBA-ESSO-ESSR (EAEE) Innsbruck consensus guidelines or to liver pathology affecting liver function. In compliance with PRISMA-ScR guidelines, systematic searches of the Embase, Web of Science, and Medline databases were conducted until October 9, 2023. Results: A total of 216 studies were included. The current applications and limitations of T1-relaxometry, magnetic resonance elastography (MRE), diffusion-weighted imaging (DWI), proton density fat fraction (PDFF), and multiparametric MRI for conducting quantitative liver assessment before hepatectomy are discussed. T1-relaxometry is primarily used for assessing liver function and predicting PHLF, whereas other qMRI techniques evaluate underlying liver disease. Nevertheless, their application in the preoperative setting remains limited. Conclusion: This review highlights the potential of qMRI techniques in preoperative assessment for liver surgery. Integration of individual qMRI techniques into multiparametric approaches holds promise for enhancing preoperative liver evaluation.

Keywords: *quantitative magnetic resonance imaging, liver function, hepatectomy*

List of Abbreviations:
ADC - Apparent Diffusion Coefficient
ALBI - Albumin-Bilirubin Score
cT1 - corrected T1
DCE - Dynamic Contrast Enhanced
DWI - Diffusion-Weighted Imaging
EAEE - E-AHPBA-ESSO-ESSR Innsbruck consensus guidelines
FLR - future liver remnant
HBS - Hepatobiliary Scintigraphy
ICG - Indocyanine Green
IVIM - Intravoxel Incoherent Motion
Ki - Hepatocellular Uptake Rate
LiMAX - liver maximum capacity test
LSR - Liver-to-Spleen Ratio
mpMRI - Multiparametric MRI
MRI - magnetic resonance imaging
MRE - Magnetic Resonance Elastography
PDFF - Proton Density Fat Fraction
PHLF - Post hepatectomy Liver Failure
Primovist - Gadolinium-ethoxybenzyl-diethylenetriamine pentaacetic acid
qMRI - quantitative magnetic resonance imaging
RE - Relative Enhancement
SI - Signal Intensity
T1rr - Relative Reduction in T1
TE - Transient Elastography
TIC - Time Intensity Curves

Introduction

Advancements in major hepatobiliary surgery have enabled more extensive and precise resection, demonstrating improved quality of life and extending life expectancy[1;2;3]. Maintaining a balance between maximizing tissue removal for successful radical resection and ensuring ample future liver remnant (FLR) is crucial to minimize the risk of post-hepatectomy liver failure (PHLF)[4]. Despite advanced preoperative and intraoperative techniques, the incidence of PHLF and subsequent death in patients with primary malignancies undergoing major liver resection remains high (8-12%)[5]. Hence, an accurate preoperative assessment of FLR function plays a critical role in the risk evaluation of PHLF, which is essential for clinical decision-making and treatment planning.

In patients without underlying liver disease and with an assumed homogeneous distribution of functional capacity, volumetric estimation of the FLR is currently the standard method for predicting preoperative risk[6]. Therefore, determination of underlying liver disease is crucial and should be addressed by additional diagnostic evaluation. Although the demand for non-tumoral liver biopsy has been reduced by the introduction of non-invasive tests and histological assessment is not indicated for the estimation of liver function, it continues to play an important role in the diagnosis and staging of underlying liver disease[7].

The E-AHPBA-ESSO-ESSR (EAEE) Innsbruck consensus guidelines highlight that a combined volumetric and functional assessment of the FLR in patients with suspected or known underlying liver disease is essential for the preoperative risk evaluation of PHLF[6]. Several methods, including Indocyanine green clearance (ICG), liver maximum capacity test (LiMAx, 13C-Methacetin Breath test), hepatobiliary scintigraphy (HBS) either with technetium-99m labelled mebrofenin or galactosyl human serum albumin are available for the quantitative assessment of liver function[8]. HBS, unlike LiMAx and ICG, evaluates regional variations in liver function, making it more applicable for defining resection margins in patients with heterogeneous distribution of function[9].

Magnetic resonance imaging (MRI) may offer an alternative approach in the current preoperative assessment for the evaluation of underlying liver disease and the assessment of liver function. Quantitative (q)MRI techniques have been developed for a more measurable evaluation of underlying liver disease and have been suggested as an alternative to liver biopsy[10]. Alternatively, several qMRI approaches based on liver-specific contrast agents such as gadoxetic acid have been developed for the assessment of liver function, though the extent to which qMRI techniques correlate with liver function remains largely unknown[11]. The development of both functional and histopathological qMRI techniques is progressing, and their integration into a multiparametric (mp)MRI approach holds significant promise for enhancing comprehensive assessment in clinical practice[12;13;14].

Given the potential of these advanced imaging techniques, we conducted a systematic review with the aim to identify qMRI techniques for the assessment of preoperative liver function, the risk assessment of PHLF, and evaluation of underlying liver disease. The findings in this review highlight the current applications and limitations of qMRI techniques individually and in combination in a mpMRI approach.

Methods

The study was conducted following the Preferred Reporting Items for Systematic Reviews and Meta-Analyses Extension for systematic reviews guidelines and was registered in the Prospective Register of Systematic Reviews[15;16]. Specifications of eligibility criteria, information sources, search strategy, selection, and data collection process, and data extraction were independently performed by two authors (FvdZ, PA).

2.1 Information sources and search strategy

A systematic literature search was conducted in collaboration with a librarian from the Amsterdam University Medical Center on October 9, 2023, using Embase, Web of Science, and Medline as search engines. Search terms 'MRI' and 'liver' were restricted to title, abstract or keywords. In addition, preoperative tests to measure liver function (section 2.1.1) or liver pathology affecting liver function (section 2.1.2) were used as a third term. Articles published between October 2013 and October 2023 were included, as MRI technology continues to rapidly evolve and older articles lose relevance. Additionally, reference lists of retrieved articles were evaluated for additional sources using backward snowballing. Endnote was used as a reference management tool and for deduplication[17].

2.2 Definition of methods to assess preoperative liver function before hepatectomy

Surgery is considered if the patient is fit, and the procedure is oncologically beneficial. Subsequently, surgical approach and FLR function will be determined. The EAEE-guidelines provide an overview of dynamic methods (ICG, LiMAx, HBS) and static blood markers (albumin-bilirubin (ALBI) and AST to Platelet Ratio Index (APRI)) to evaluate liver function and PHLF risk.

2.3 Definition of liver pathology affecting liver function

The ability of the remaining hepatocytes to regenerate is crucial for restoring ample function. Hence, the preoperative assessment for hepatectomy requires a precise understanding of the underlying liver diseases that lead to liver pathology affecting liver function. The EAEE-guidelines mention fibrosis, steatosis, and liver injuries from drugs or chemotherapy potentially impair liver function and regeneration. Liver biopsy is recommended to stage and differentiate liver pathology in patients with suspected or known underlying liver disease. Additionally, liver stiffness measurement with transient elastography (TE) should be considered for risk evaluation in these patients[18]. Therefore, the mentioned pathologies, biopsy and TE were included in the literature search[6].

2.4 Study selection procedure

Articles were included if they reported qMRI techniques compared with dynamic functional tests and static blood markers

to assess liver function or were deemed predictive of PHLF. Articles were included if they reported qMRI techniques that were compared to histopathological scoring systems to assess liver pathology. Exclusion criteria were as follows: (1) non-English articles; (2) no full text, reviews, commentary, conference abstracts, reports, protocols and guidelines; (3) animal, phantom or ex vivo research; (4) humans < 18 years; (5) functional test used as a reference not mentioned in the EAEE-guideline; (6) MRI used as a reference standard. Additional deduplication and title/abstract study selection were independently performed by two authors in a systematic review collaboration platform[19]. Conflicting selections were discussed per study till consensus was met, yielding the studies selected for inclusion.

2.5   Synthesis of results
The included articles were sorted into categories according to qMRI techniques. The identification of existing systematic reviews evaluating the techniques described in the defined groups were separately conducted. Full-text screening of articles was performed when topics were not covered by existing systematic reviews.

Results
3.1   Search results
The search across three databases yielded 10,889 articles. After removing duplicates in Endnote and Rayyan, 7,373 articles were screened by title and abstract. 216 articles were included after title and abstract screening. Figure 1 illustrates the selection process according to the PRISMA-ScR guidelines. MRI techniques were classified into T1-relaxometry, diffusion-weighted imaging (DWI), magnetic resonance elastography (MRE), proton density fat fraction (PDFF) and mpMRI. T1-relaxometry studies predominantly focused on the assessment of liver function, whereas the majority of other qMRI techniques focused on histopathological outcomes (Fig 2a). 22 studies included surgical patients, mostly investigating the relationship with T1-relaxometry and the assessment preoperative liver function. A total of 16 studies explored qMRI as a potential tool for prediction of PHLF. Of these, 15 employed T1-relaxometry and one study used MRE.

3.2   T1-relaxometry
A total of 87 articles and three systematic reviews on T1-relaxometry were included in this category. T1-relaxometry involves measuring the longitudinal or spin-lattice relaxation time of hepatic tissue, which depends on the transfer of energy to the surrounding tissue. The amount of energy transferred varies with different tissue characteristics, thereby generating contrast in images. This effect can be enhanced using liver-specific contrast agents such as Gadolinium-ethoxy benzyl- diethylenetriamine pentaacetic acid (Gd-EOB-DTPA; Primovist®). Contrast agents are taken up and excreted by hepatocytes, reaching a maximum accumulation in the hepatobiliary phase approximately 20 minutes after administration. Paramagnetic properties of these contrast agents reduce T1-relaxation times, thus enhancing signal intensity (SI). Based on this effect several indices were established.
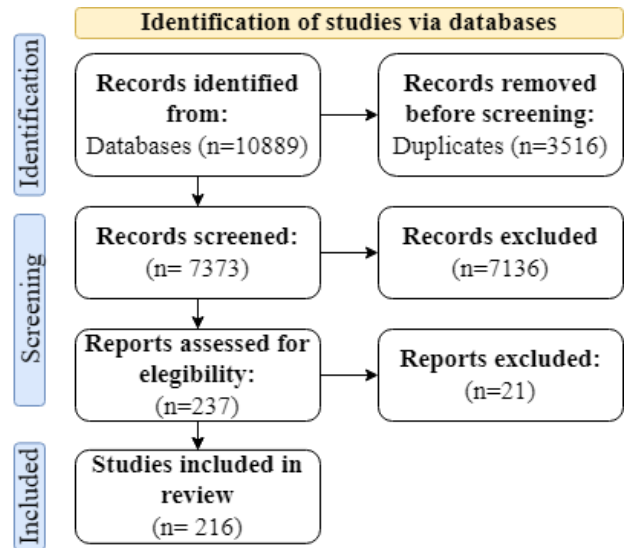

Figure 1: Identification of included studies and classification of selected articles into quantitative MRI groups. T1; T1-relaxometry, DWI; Diffusion weighted imaging, SWI; susceptibility weighted imaging, MRE; magnetic resonance elastography, PDFF; proton density fat fraction
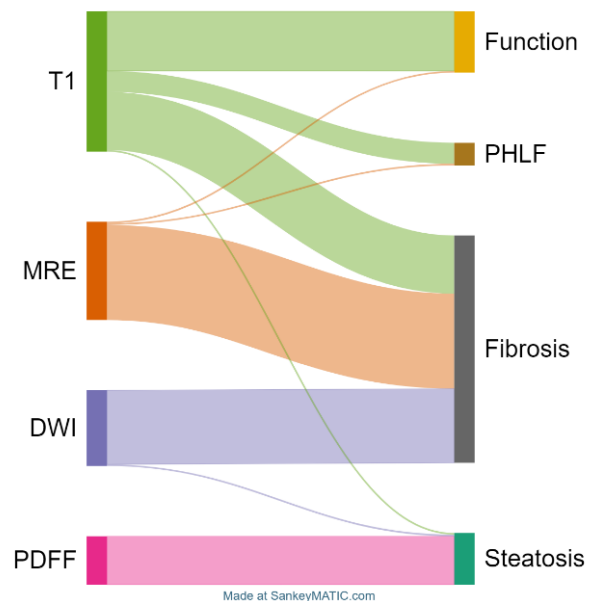

Figure 2: Sankey diagram illustrating the relationships between qMRI and clinical outcomes in liver disease assessment. DWI; diffusion weighted imaging, PDFF; proton density fat fraction, MRE; magnetic resonance elastography, PHLF; posthepatectomy liver failure

3.2.1   Contrast enhanced indices
SI and relaxometry-based indices (Table 1) estimate liver function by measuring SI and relaxation rates before and after contrast injection. This uptake of contrast agents is indicative of hepatocyte excretion. In cases where liver function may be heterogeneous, whole liver measurements can provide information about the distribution of functional capacity. A meta-analysis comparing the most commonly used indices (Table 1. Relative enhancement (RE), liver to spleen

3

ratio (LSR), liver to muscle ratio and T1 relaxation rate (T1rr)) with ICG demonstrated moderate correlations [20]. However, additional studies not included in this meta-analysis showed moderate to strong correlations, which also applied to the less frequently used indices [21;22;23;24]. Moreover, SI-histogram analysis enabled the differentiation between groups with high (> 20) and low (< 20) ICG clearance [25]. Among SI-based and relaxometry-based indices, the T1rr index exhibited the strongest correlation ($r = 0.83$) with ICG clearance [22]. Integrating liver volume into these indices resulted in no or only marginal improvement in correlation coefficients with ICG clearance [26]. Comparative studies of RE and T1rr with LiMAX revealed moderate correlations for RE and strong correlations for T1rr [27;28;29;30]. A study by Wang et al., examined multiple correlations between HBS and SI-indices, demonstrating considerable variability in the comparisons. A derivative of HBS demonstrated a strong correlation with LSR, while the clinically used HBS value showed moderate correlation [31]. Additionally, moderate correlations with the hepatocellular uptake index were observed, whereas Geisel et al. found strong correlations in the remnant liver lobe [32]. In accordance with previous findings, the results indicated that RE and HBS exhibited moderate correlations [33]. Mori et al., measured the LSR one hour after contrast injection and found a strong correlation with HBS parameters [34]. In addition to dynamic comparisons, static serum markers were correlated to T1-values to assess liver uptake function. Included studies consistently demonstrate a moderate negative correlation between the ALBI score and liver enhancement ratios [35;36;37;38]. Moreover, a combination of T1rr with height, weight, and liver volume demonstrated a moderately negative correlation with the ALBI score [39].

A recent systematic review reported on the potential of contrast-enhanced T1-relaxometry to distinguish PHLF from nonPHLF [40]. Subsequently, a study was published which predicted PHLF with LSR, yielding results consistent with the findings of the systematic review [41]. However, further studies using prospective, large-scale samples and standardized parameters are required to confirm these findings and to establish clinically applicable cut-off values [40;41].

Besides the potential of T1-relaxometry to estimate liver function and predict PHLF, one systematic review and 25 studies focussed on the correlation between T1-relaxometry and fibrosis. Fibrosis results in a reduction in tissue perfusion and permeability, which potentially makes contrast enhanced T1-relaxometry an appropriate tool for quantification. Moreover, estimation per voxel may be valuable in resection planning as it provides insights into the distribution of fibrotic tissue throughout the liver. The included systematic review and meta-analysis showed a good diagnostic efficacy for several gadoxetic acid-enhanced MRI based SI and relaxometry based indices in the staging of liver fibrosis [42]. Several articles demonstrated good to excellent diagnostic accuracy for the detection of no and mild levels of fibrosis (F0-F2). Alternatively, several articles showed good to excellent diagnostic accuracy for detection of low and high levels of fibrosis when multiple fibrosis stages where combined into groups, representing a more binary division [43;44;45;46]. Nevertheless, the diagnostic performance of MRE for fibrosis was found superior to any T1 based method [47;48]. Additionally, T1 relaxation times may be affected by inflammation, the presence of iron and acute elevation in liver enzymes and bile parameters [49;50;51]. Failing to account for these confounders may affect diagnostic accuracy.

3.2.2 Dynamic contrast enhanced

In contrast to the previously mentioned T1-techniques, dynamic contrast-enhanced (DCE)-MRI enables the measurement of changes in tissue signal intensity over time. Seven studies were included in the current review, which reported on DCE-MRI. Four of these studies focused on liver function, three assessed the correlation with fibrosis. Time intensity curves (TIC) of the contrast agent dynamics provide a visual representation of the hepatic uptake over time. Pharmacokinetic models can be applied to extract biological parameters from TIC. The maximum slope of increase, derived from the TIC, was compared to HBS to estimate remnant liver function. However, none of the results were found to be statistically significant [33]. The employed PK models differed in terms of number of inputs and compartments, which makes direct comparisons between studies challenging. Studies indicate that hepatic perfusion and hepatocellular uptake rate (Ki) can effectively quantify liver function, showing strong correlations with ICG clearance [52;53]. Moreover, hepatic uptake and excretion of technetium-labelled mebrofenin in HBS and Primovist in DCE-MRI use similar transporters and show a strong correlation with remnant liver function ($r = 0.89$), suggesting the potential of DCE-MRI as an alternative to HBS [33]. Nevertheless, moderate correlations were found in comparison to technetium-99 m galactosyl human serum albumin [54].

Four studies were included in the analysis, which quantified fibrosis with DCE-MRI. DCE-MRI parameters, including Ki and TIC-derived values, demonstrate significant correlations with fibrosis stages, with AUROC values between 0.71 and 0.84 indicating strong diagnostic performance [55;56]. However, a Ki correlation of R = -0.55 reported by Juluru suggests a moderate relationship [57]. No statistically significant correlation was observed between Ki and the fibrosis stages determined by TE [58].

3.2.3 Non-contrast

Non-contrast T1-mapping and T1-rho techniques allow for the measurement of liver properties without the need for contrast agents. Non-contrast T1-mapping quantifies the T1 relaxation time of tissues by acquiring images at different inversion times. Although no correlation with T1-mapping and ALBI to estimate liver function has been identified [59]. T1rho measures T1 relaxation with a continuous radio frequency pulse. This technique is sensitive to the movement of low-frequency protons, enabling the detection of changes in macromolecules and disrupted proton movement, which are characteristic of fibrosis. Studies have demonstrated that T1rho correlates strongly with the severity of liver fibrosis even in the presence of fat, when compared with histological scoring systems and TE [60;61;62;63]. However, differentiating early stages of fibrosis (F0 vs. F1-2) was not possible with

Abbreviation	Meaning	Formula
RE	Relative Enhancement	$RE = \frac{SI_{post} - SI_{pre}}{SI_{pre}} \times 100$
LSR	Liver-to-Spleen Ratio	$LSR = \frac{SI_{\text{liver}}}{SI_{\text{spleen}}}$
LSM	Liver-to-Muscle Ratio	$LSM = \frac{SI_{\text{liver}}}{SI_{\text{muscle}}}$
HUI	Hepatic Uptake Index	$HUI = \frac{SI_{\text{liver}}}{SI_{\text{liver}} + SI_{\text{background}}}$
rHUI	Relative Hepatic Uptake Index	$rHUI = V_l \left(\frac{SI_{\text{liver, 20}}}{SI_{\text{spleen, 20}}} - 1 \right)$
T1rr	T1 Relaxation Rate	$T1rr = \frac{1}{T1}$
ΔLSR	Increase Rate of Liver-to-Spleen Ratio	$\Delta LSR = \frac{LSR_{post} - LSR_{pre}}{LSR_{pre}} \times 100$
ΔLSM	Increase Rate of Liver-to-Muscle Ratio	$\Delta LSM = \frac{LSM_{post} - LSM_{pre}}{LSM_{pre}} \times 100$
ΔR1	Change in Relaxation Rate	$\Delta R1 = \frac{1}{T1_{\text{post}}} - \frac{1}{T1_{\text{pre}}}$

Table 1: Summary of T1-relaxometry and signal intensity indices

T1rho[64].

3.3 DWI

In DWI, the MRI signal is sensitized to random Brownian motion of water molecules within a tissue voxel. Differences in organization of structure of the liver parenchyma affect the diffusion of water and contribute to image contrast. By measuring the signal at different diffusion-weightings, the apparent diffusion coefficient (ADC) can be calculated. Intravoxel incoherent motion (IVIM) is an extended model that employs a bi-exponential rather than a mono-exponential DWI model. It has the ability to quantify perfusion and diffusion separately, providing additional parameters such as the perfusion fraction, true diffusion coefficient, and pseudo-diffusion coefficient.

One study used a complex DWI model that accounts for the non-gaussian distribution of water to assess liver function directly and found moderate correlations when compared to ICG and ALBI[65]. The remaining 31 studies, including two systematic reviews, focused on the staging of fibrosis using DWI or extended DWI models.

Results from a systematic review suggest that DWI can accurately differentiate between stages of liver fibrosis compared with histological fibrosis scoring[66]. Studies not included in the systematic review have shown that ADC values can distinguish between fibrotic and non-fibrotic groups, and ADCs decrease significantly as fibrosis increases[67;68;69;70;71;72;73;74;75;76;77;78;79;80;81]. However, other studies have reported a decrease in ADC with increasing fibrosis that was not statistically significant[78;82]. Moreover, the ability of DWI to distinguish between different fibrosis stages varies across studies, particularly between intermediate stages[68;77;80;81]. Compared to TE, moderate correlations were found[83;84].

A meta-analysis conducted by Ye et al. (2020) highlighted the diagnostic potential of IVIM for both detecting and staging liver fibrosis, with AUC values of 0.862 for $\geq$ F1, 0.883 for $\geq$ F2, 0.886 for $\geq$ F3, and 0.899 for F4[85]. Subsequent studies have confirmed these results[86;87;88]. Nevertheless,

considerable heterogeneity was observed within the included studies[85]. Furthermore, studies indicated that values were not reproducible due to confounding factors[89;90].

The efficacy of advanced diffusion models, including diffusion kurtosis imaging, diffusion tensor imaging, and the distribution diffusion coefficient, has been evaluated for the detection and staging of liver function and fibrosis[91;92;93;94]. However, two studies that used diffusion kurtosis imaging and distribution diffusion coefficient demonstrated a diagnostic enhancement over DWI and IVIM in the staging of fibrosis[93;94].

3.4 PDFF

A total of 22 articles were included that reported on PDFF, a non-invasive modality for the measurement of hepatic fat fractions. Eleven of the included articles were discussed in recent systematic reviews and demonstrated the high diagnostic accuracy of PDFF in the quantitative grading of hepatic steatosis when compared with histological assessment as reference standard[95;96;97;98]. Liver biopsy was found to overestimate steatosis grade compared to PDFF[99;100;101]. Moreover, PDFF showed high diagnostic accuracy for hepatic fat fractions and outperformed several other imaging modalities, such as magnetic resonance spectroscopy and TE[102;103;104;105;106]. Comparative results were found in the remaining included articles[107;108;109;110;111]. Particularly high diagnostic accuracy was observed for moderate and severe grade steatosis[108;112]. Potential confounding factors, such as iron overload, inflammation and fibrosis can be mitigated in PDFF measurements when complemented with multi-echo sequences and T2* corrections[113;114;115;116].

3.5 MRE

A total of 52 articles were included that reported on MRE, which quantifies liver stiffness or elasticity by transmitting shear waves using an external wave generator and a passive driver. 25 of the included articles in the present study were discussed in recent systematic reviews.

One systematic review reported on liver stiffness assessed by MRE as a prognostic value for postoperative outcomes. How-

ever, PHLF was not explicitly identified as a primary outcome measure[117]. Two studies have demonstrated that hepatic stiffness values may be predictive of PHLF[118;119]. Another study directly compared MRE measurements to ICG clearance in hepatocellular carcinoma patients, demonstrating a correlation between increased non-tumour liver stiffness and higher ICG levels. This suggests that MRE may have potential for assessing functional reserve in hepatocellular carcinoma patients[120].

The majority of systematic reviews reported on the staging of fibrosis and cirrhosis across various liver conditions. These consistently demonstrated the excellent diagnostic accuracy of MRE for significant (F0-1 vs. F2-4) and advanced (F0-2 vs F3-4) fibrosis and cirrhosis stages (F0-3 vs F4), in comparison to biopsy[96;121;122;123;124;125;126;127;128;129;130]. In addition to the systematic reviews, 26 articles provide a comparison of MRE with histopathological scoring systems and blood markers to assess fibrosis. Compared to histopathology, MRE demonstrated equivalent or superior performance in the detection of significant fibrosis, consistent with the findings of the discussed systematic reviews[104;111;120;131;132 133;134;135;136;137;138;139]. Furthermore, MRE also showed improved diagnostic accuracy compared to serum markers and other qMRI methods (DWI, DCE, T1-relaxometry and T2-relaxometry)[134;137;140;141;142;143;144;145].

Remaining articles present technical conclusions that demonstrate the comparable performance of different 2D and 3D acquisition methods, despite the potential to image the entire liver with 3D MRE[146;147;148]. However, 3D-MRE can detect early necroinflammation and distinguish it from liver fibrosis[149]. Clinically, MRE provides an accurate, reproducible, and non-invasive assessment of liver fibrosis, regardless of the aetiology, and is not limited by obesity or ascites[125;150].

3.6 mpMRI

MpMRI integrates multiple individual qMRI techniques into a single acquisition, which is hypothesized to mitigate some of the limitations and confounders associated with individual techniques. To date, there have been no studies reporting on the use of mpMRI for the preoperative assessment of liver function or for the risk evaluation of PHLF. Furthermore, no studies compared mpMRI to dynamic liver function tests.

Several studies have reported on mpMRI for the assessment of underlying liver disease. One study reported promising diagnostic performance of mpMRI for diagnosing and staging steatosis, fibrosis and disease activity in non-alcoholic fatty liver disease and analysed several imaging parameters from magnetic resonance spectroscopy, PDFF, IVIM and MRE[151]. Feier et al., Combined DWI, susceptibility-weighted imaging and RE parameters and demonstrated excellent diagnostic performance for staging the severity of liver fibrosis[152]. Another study combined corrected (c)T1, T2*- relaxometry, and PDFF, and effectively evaluated fibrosis, hemosiderosis, and steatosis, respectively[153]. The three studies discuss the potential of mpMRI as substitute for liver biopsy. However, in these studies no combination of individual outcomes were analysed in a multivariate regression to investigate the relationship between parameters. McDonald et al. identified a significant correlation between cT1 values and fibrosis across different inflammation severity levels in a multivariate analysis[154]. An additional study found that combining several qMRI techniques in a mpMRI protocol with volume predicts postoperative outcomes, suggesting its potential for future personalized treatment[155].

Discussion

This review was conducted to investigate the potential role of qMRI techniques for the preoperative assessment liver function, the ability to predict PHLF and for the evaluation of underlying liver disease either individually or in a mpMRI approach.

Results demonstrate the promising role of T1-relaxometry in the assessment of preoperative liver function and prediction of PHLF, however methodological variability and small study cohorts limit standardization and complicates reproducibility. Despite their potential to be combined, no studies have explored a mpMRI approach to assess liver function or predict PHLF. MRE, DWI and PDFF were employed primarily for the diagnosis and staging of underlying liver disease. Nevertheless, a direct comparison between the influence of underlying liver disease on liver function was not determined.

Reviews have reported on the role of contrast-enhanced T1-relaxometry in measuring liver function[11;156]. Unal et al. indicated the use of SI indices for identifying different liver dysfunction patterns in patients with chronic liver disease[156]. However, these reviews did not address the use of DCE for measuring liver function and other qMRI techniques for assessing parenchymal status. Moreover, single blood markers, Child-Pugh and model for end-stage liver disease clinical grading systems have been used as surrogates for predicting PHLF. However, these lack precision in determining the perioperative risk of PHLF, as defined by the EAEE-guidelines and were therefore excluded from our review[6].

Despite the promising results of SI-indices to assess liver function, it should be acknowledged that contrast-enhanced measurements primarily reflect the hepatic uptake and bile excretion of hepatocytes. Moreover, SI values are affected by paramagnetic field inhomogeneities due to technical parameters, rendering them non-absolute and therefore semi-quantitative. Therefore, deriving indices from relaxation rates is more reliable than relying on a single SI measurement. However, direct correlation between the uptake of Primovist and T1 relaxation rates due to the influence of physiological and aetiology of underlying liver disease. Moreover, correct determination of the hepatobiliary phase is not standardized between centres and still varies significantly between patients[157;158;159]. Continuous measurement of contrast uptake with DCE is regarded as a more quantitative approach, also given its ability to extract more intricate biological parameters. However, implementation of DCE has not yet been feasible due to the complexity of pharmacokinetic models and lack of standardization[66].

T1-relaxometry and MRE have been applied to predict major post-operative outcomes. However, the correlation between T1-relaxometry and PHLF remains unclear due to

small study groups and the low incidence of PHLF. To establish a clear correlation between T1-relaxometry and PHLF, larger-scale studies with more diverse patient populations are necessary. While liver stiffness has been demonstrated to predict PHLF, it is predominantly evaluated through TE[6]. Nevertheless, MRE demonstrates superior diagnostic performance, a lower technical failure rate, applicability in patients with obesity and ascites, and better reproducibility in measuring liver stiffness compared to TE[160;161].

MRE, DWI, and T1 are all effective methods for assessing fibrosis, with MRE demonstrating the highest accuracy. However, MRE is limited by the need for specialized hardware. Numerous factors related to tissue composition affect relaxation times, complicating interpretation of measurements. For example, the presence of fat can influence DWI imaging and iron overload complicates MRE, rendering it non-diagnostic in patients with steatosis or hemosiderosis respectively[161;162]. Moreover, while PDFF is an accurate method for quantifying liver fat, it may also be influenced by the presence of iron.

Challenges posed by confounders make qMRI complex, but they also increase the potential for success with mpMRI over other modalities if these interactions can be accurately interpreted[163]. T2*-relaxometry and advanced MRI-PDFF techniques are currently employed in an mpMRI approach for the quantification of iron and the assessment of regional liver fat content, respectively. While another commercially available product also offers quantification of fibrosis and inflammation, there are currently no studies that have incorporated qMRI techniques for liver function assessment in an mpMRI approach. 'Liver health,' as measured by the LiverMultiScan (Perspectum, Oxford, UK), has been proposed as a potential pre-operative method to predict the risk of PHLF[155]. However, while the LiverMultiScan has been validated against liver biopsy, it is crucial to recognize the limitations of biopsy in the context of preoperative liver function assessment and subsequent risk of PHLF[12]. The HepaT1ca trial would potentially benefit from correlations with validated methods for the assessment of liver function to enhance its clinical application.

PDFF and MRE are employed in clinical practice, demonstrating the feasibility of qMRI in routine practice. However, challenges such as variability across scanners, complex interpretation, and the lack of standardized protocols hinder their widespread adoption. Furthermore, other qMRI techniques are currently limited to research settings and cannot be implemented in clinical practice due to the predominant use of in-house analysis within single-center studies, which impedes comparability across different studies. To ensure reproducibility and effective implementation of qMRI in preoperative settings, future multi-center studies are needed. Adoption of guidelines from organisations such as the Quantitative Imaging Biomarker Alliance and the National Cancer Institute Quantitative Imaging Network could standardise protocols, thereby providing accurate liver function quantification in preoperative settings[163].

Despite the promising potential of qMRI in preoperative liver assessment, limitations within this review should be acknowledged. The review primarily focused on fundamentals of qMRI techniques a and their application, omitting technical aspects. However, the ongoing development of qMRI through technical innovations is essential for expanding its clinical applicability. Additionally, various underlying liver pathologies and comparative techniques within our methodology introduce complexities in synthesizing results and drawing definitive conclusions.

Conclusion

Identified techniques, including T1-relaxometry, DWI, PDFF and MRE offer valuable insights in assessment of liver function, prediction of PHLF and evaluation of parenchymal status. Integration of individual qMRI techniques into multi-parametric approaches holds promise for enhancing preoperative liver evaluation. However, further studies are essential to establish more robust correlations between qMRI techniques and dynamic liver function tests, as well as to identify the role of underlying liver disease on liver function. Additionally, standardizing imaging protocols and conducting large-scale multi-center studies are required in order to enhance diagnostic accuracy and clinical applicability.

References

1. Wee IJY, Syn N, Lee LS, Tan SS, Chiow AKH. A systematic review and meta-analysis on the quality of life after hepatic resection. HPB (Oxford). 2020;22(2):177-86.
2. Liu W, Wang K, Bao Q, Sun Y, Xing BC. Hepatic resection provided long-term survival for patients with intermediate and advanced-stage resectable hepatocellular carcinoma. World J Surg Oncol. 2016;14:62.
3. Andreou A, Knitter S, Schmelzle M, Kradolfer D, Maurer MH, Auer TA, et al. Recurrence at surgical margin following hepatectomy for colorectal liver metastases is not associated with R1 resection and does not impact survival. Surgery. 2021;169(5):1061-8.
4. Guglielmi A, Ruzzenente A, Conci S, Valdegamberi A, Iacono C. How much remnant is enough in liver resection? Dig Surg. 2012;29(1):6-17.
5. Soreide JA, Deshpande R. Post hepatectomy liver failure (PHLF) - Recent advances in prevention and clinical management. Eur J Surg Oncol. 2021;47(2):216-24.
6. Primavesi F, Maglione M, Cipriani F, Denecke T, Oberkofler CE, Starlinger P, et al. E-AHPBA-ESSO-ESSR Innsbruck consensus guidelines for preoperative liver function assessment before hepatectomy. Br J Surg. 2023;110(10):1331-47.
7. Neuberger J, Patel J, Caldwell H, Davies S, Hebditch V, Hollywood C, et al. Guidelines on the use of liver biopsy in clinical practice from the British Society of Gastroenterology, the Royal College of Radiologists and the Royal College of Pathology. Gut. 2020;69(8):1382-403.
8. Tomassini F, Giglio MC, De Simone G, Montalti R, Troisi RI. Hepatic function assessment to predict post-hepatectomy liver failure: what can we trust? A systematic review. Updates in surgery. 2020;72:925-38.
9. Rassam F, Olthof PB, Bennink RJ, van Gulik TM. Current Modalities for the Assessment of Future Remnant Liver Function. Visc Med. 2017;33(6):442-8.
10. Neuberger J, Cain O. The Need for Alternatives to Liver Biopsies: Non-Invasive Analytics and Diagnostics. Hepat

Med. 2021;13:59-69.

11. Rio Bartulos C, Senk K, Schumacher M, Plath J, Kaiser N, Bade R, et al. Assessment of Liver Function With MRI: Where Do We Stand? Front Med (Lausanne). 2022;9:839919.

12. Mole DJ, Fallowfield JA, Kendall TJ, Welsh F, Semple SI, Bachtiar V, et al. Study protocol: HepaT1ca - an observational clinical cohort study to quantify liver health in surgical candidates for liver malignancies. BMC Cancer. 2018;18(1):890.

13. Li C, Liu H, Wang J, Li X, Cui T, Wang R, et al. Multiparametric MRI combined with liver volume for quantitative evaluation of liver function in patients with cirrhosis. Diagn Interv Radiol. 2022;28(6):547-54.

14. Troelstra MA, Witjes JJ, van Dijk AM, Mak AL, Gurney-Champion O, Runge JH, et al. Assessment of Imaging Modalities Against Liver Biopsy in Nonalcoholic Fatty Liver Disease: The Amsterdam NAFLD-NASH Cohort. J Magn Reson Imaging. 2021;54(6):1937-49.

15. Page MJ, McKenzie JE, Bossuyt PM, Boutron I, Hoffmann TC, Mulrow CD, et al. The PRISMA 2020 statement: An updated guideline for reporting systematic reviews. J Clin Epidemiol. 2021;134:178-89.

16. Tricco AC, Lillie E, Zarin W, O'Brien KK, Colquhoun H, Levac D, et al. PRISMA Extension for Scoping Reviews (PRISMA-ScR): Checklist and Explanation. Ann Intern Med. 2018;169(7):467-73.

17. Gotschall T. EndNote 20 desktop version. J Med Libr Assoc. 2021;109(3):520-2.

18. Tapper EB, Lok ASF. Use of Liver Imaging and Biopsy in Clinical Practice. N Engl J Med. 2017;377(23):2296-7.

19. Ouzzani M, Hammady H, Fedorowicz Z, Elmagarmid A. Rayyan-a web and mobile app for systematic reviews. Syst Rev. 2016;5(1):210.

20. Ai X, Wang H, Yang Y, Feng Y, Xie X, Zhao X, et al. Four indices on Gd-EOB-DTPA-enhanced MRI can estimate liver functional reserve compared to ICG-R15: A systematic review and meta-analysis. Clin Imaging. 2023;102:1-8.

21. Eiras-Araujo AL, Parente DB, da Silva AC, da Motta Rezende GF, Mendes GB, Luiz RR, et al. Relative enhancement index can be used to quantify liver function in cirrhotic patients that undergo gadoxetic acid-enhanced MRI. Eur Radiol. 2023;33(7):5142-9.

22. Haimerl M, Schlabeck M, Verloh N, Zeman F, Fellner C, Nickel D, et al. Volume-assisted estimation of liver function based on Gd-EOB-DTPA-enhanced MR relaxometry. Eur Radiol. 2016;26(4):1125-33.

23. Wang HQ, Jin KP, Zeng MS, Chen CZ, Rao SX, Ji Y, et al. Assessing liver fibrosis in chronic hepatitis B using MR extracellular volume measurements: Comparison with serum fibrosis indices. Magn Reson Imaging. 2019;59:39-45.

24. Bi XJ, Zhang XQ, Zhang T, Xu L, Huang AN, Liu MT, et al. Quantitative assessment of liver function with hepatocyte fraction: Comparison with T1 relaxation-based indices. Eur J Radiol. 2021;141:109779.

25. Asayama Y, Nishie A, Ishigami K, Ushijima Y, Takayama Y, Okamoto D, et al. Histogram analysis of noncancerous liver parenchyma on gadoxetic acid-enhanced MRI: predictive value for liver function and pathology. Abdom Radiol (NY). 2016;41(9):1751-7.

26. Haimerl M, Verloh N, Zeman F, Fellner C, Nickel D, Lang SA, et al. Gd-EOB-DTPA-enhanced MRI for evaluation of liver function: Comparison between signal-intensity-based indices and T1 relaxometry. Sci Rep. 2017;7:43347.

27. Haimerl M, Probst U, Poelsterl S, Beyer L, Fellner C, Selgrad M, et al. Hepatobiliary MRI: Signal intensity based assessment of liver function correlated to (13)C-Methacetin breath test. Sci Rep. 2018;8(1):9078.

28. Probst U, Sieron D, Bruenn K, Fuhrmann I, Verloh N, Stroszczynski C, et al. Efficacy of dynamic enhancement effects on Gd-EOB-DTPA-enhanced MRI for estimation of liver function assessed by 13C- Methacetin breath test. Clin Hemorheol Microcirc. 2018;70(4):595-604.

29. Verloh N, Fuhrmann I, Fellner C, Nickel D, Zeman F, Kandulski A, et al. Quantitative analysis of liver function: 3D variable-flip-angle versus Look-Locker T1 relaxometry in hepatocyte-specific contrast-enhanced liver MRI. Quant Imaging Med Surg. 2022;12(4):2509-22.

30. Theilig D, Tsereteli A, Elkilany A, Raabe P, Ludemann L, Malinowski M, et al. Gd-EOB-DTPA-enhanced MRI T1 relaxometry as an imaging-based liver function test compared with (13)C-methacetin breath test. Acta Radiol. 2020;61(3):291-301.

31. Wang Q, Brismar TB, Gilg S, Jonas E, Nilsson H, Tzortzakakis A, et al. Multimodal perioperative assessment of liver function and volume in patients undergoing hepatectomy for colorectal liver metastasis: a comparison of the indocyanine green retention test, (99m)Tc mebrofenin hepatobiliary scintigraphy and gadoxetic acid enhanced MRI. Br J Radiol. 2022;95(1139):20220370.

32. Geisel D, Ludemann L, Froling V, Malinowski M, Stockmann M, Baron A, et al. Imaging-based evaluation of liver function: comparison of (9)(9)mTc-mebrofenin hepatobiliary scintigraphy and Gd-EOB-DTPA-enhanced MRI. Eur Radiol. 2015;25(5):1384-91.

33. Rassam F, Zhang T, Cieslak KP, Lavini C, Stoker J, Bennink RJ, et al. Comparison between dynamic gadoxetate-enhanced MRI and (99m)Tc-mebrofenin hepatobiliary scintigraphy with SPECT for quantitative assessment of liver function. Eur Radiol. 2019;29(9):5063-72.

34. Mori H, Machimura H, Iwaya A, Baba M, Furuya K. Comparison of liver scintigraphy and the liver-spleen contrast in Gd-EOB-DTPA-enhanced MRI on liver function tests. Sci Rep. 2021;11(1):22472.

35. Beer L, Mandorfer M, Bastati N, Poetter-Lang S, Tamandl D, Stoyanova DP, et al. Inter- and intra-reader agreement for gadoxetic acid-enhanced MRI parameter readings in patients with chronic liver diseases. Eur Radiol. 2019;29(12):6600-10.

36. Ippolito D, Famularo S, Giani A, Orsini EB, Pecorelli A, Pinotti E, et al. Estimating liver function in a large cirrhotic cohort: Signal intensity of gadolinium-ethoxybenzyl-diethylenetriamine penta-acetic acid-enhanced MRI. Dig Liver Dis. 2019;51(10):1438-45.

37. Ocal O, Peynircioglu B, Loewe C, van Delden O, Vandecaveye V, Gebauer B, et al. Correlation of liver enhancement in gadoxetic acid-enhanced MRI with liver functions: a multicenter-multivendor analysis of hepatocellular carcinoma patients from SORAMIC trial. Eur Radiol. 2022;32(2):1320-9.

38. Takatsu Y, Kobayashi S, Miyati T, Shiozaki T. Hepatobiliary phase images using gadolinium-ethoxybenzyl-diethylenetriamine penta-acetic acid-enhanced MRI as an imaging surrogate for the albumin-bilirubin grading system. Eur J Radiol. 2016;85(12):2206-10.

39. Rio Bartulos C, Senk K, Bade R, Schumacher M, Kaiser N, Plath J, et al. Using AI and Gd-EOB-DTPA-enhanced MR imaging to assess liver function, comparing the MELIF score with the ALBI score. Sci Rep. 2023;13(1):13121.

40. Wang Q, Wang A, Sparrelid E, Zhang J, Zhao Y, Ma K, Brismar TB. Predictive value of gadoxetic acid-enhanced MRI

for posthepatectomy liver failure: a systematic review. Eur Radiol. 2022;32(3):1792-803.

41. Kudo M, Gotohda N, Sugimoto M, Konishi M, Takahashi S, Kobayashi S, Kobayashi T. The Assessment of Regional Liver Function Before Major Hepatectomy Using Magnetic Resonance Imaging. Am Surg. 2022;88(9):2353-60.

42. Yang D, Li D, Li J, Yang Z, Wang Z. Systematic review: The diagnostic efficacy of gadoxetic acid-enhanced MRI for liver fibrosis staging. Eur J Radiol. 2020;125:108857.

43. Keller S, Aigner A, Zenouzi R, Kim AC, Meijer A, Weidemann SA, et al. Association of gadolinium-enhanced magnetic resonance imaging with hepatic fibrosis and inflammation in primary sclerosing cholangitis. PLoS One. 2018;13(3):e0193929.

44. Feier D, Balassy C, Bastati N, Stift J, Badea R, Ba-Ssalamah A. Liver fibrosis: histopathologic and biochemical influences on diagnostic efficacy of hepatobiliary contrast-enhanced MR imaging in staging. Radiology. 2013;269(2):460-8.

45. Tokorodani R, Kume T, Daisaki H, Hayashi N, Iwasa H, Yamagami T. Combining 99mTc-GSA single-photon emission-computed tomography and Gd-EOB-DTPA-enhanced magnetic resonance imaging for staging liver fibrosis. Medicine (Baltimore). 2023;102(7):e32975.

46. Ou HY, Bonekamp S, Bonekamp D, Corona-Villalobos CP, Torbenson MS, Geiger B, Kamel IR. MRI arterial enhancement fraction in hepatic fibrosis and cirrhosis. AJR Am J Roentgenol. 2013;201(4):W596-602.

47. Hoffman DH, Ayoola A, Nickel D, Han F, Chandarana H, Shanbhogue KP. T1 mapping, T2 mapping and MR elastography of the liver for detection and staging of liver fibrosis. Abdom Radiol (NY). 2020;45(3):692-700.

48. Kim SW, Lee JM, Park S, Joo I, Yoon JH, Chang W, Kim H. Diagnostic Performance of Spin-Echo Echo-Planar Imaging Magnetic Resonance Elastography in 3T System for Noninvasive Assessment of Hepatic Fibrosis. Korean J Radiol. 2022;23(2):180-8.

49. Bastati N, Feier D, Wibmer A, Traussnigg S, Balassy C, Tamandl D, et al. Noninvasive differentiation of simple steatosis and steatohepatitis by using gadoxetic acid-enhanced MR imaging in patients with nonalcoholic fatty liver disease: a proof-of-concept study. Radiology. 2014;271(3):739-47.

50. Breit HC, Block KT, Winkel DJ, Gehweiler JE, Henkel MJ, Weikert T, et al. Evaluation of liver fibrosis and cirrhosis on the basis of quantitative T1 mapping: Are acute inflammation, age and liver volume confounding factors? Eur J Radiol. 2021;141:109789.

51. Hoad CL, Palaniyappan N, Kaye P, Chernova Y, James MW, Costigan C, et al. A study of T(1) relaxation time as a measure of liver fibrosis and the influence of confounding histological factors. NMR Biomed. 2015;28(6):706-14.

52. Cao Y, Wang H, Johnson TD, Pan C, Hussain H, Balter JM, et al. Prediction of liver function by using magnetic resonance-based portal venous perfusion imaging. Int J Radiat Oncol Biol Phys. 2013;85(1):258-63.

53. Simeth J, Johansson A, Owen D, Cuneo K, Mierzwa M, Feng M, et al. Quantification of liver function by linearization of a two-compartment model of gadoxetic acid uptake using dynamic contrast-enhanced magnetic resonance imaging. NMR Biomed. 2018;31(6):e3913.

54. Saito K, Ledsam J, Sourbron S, Hashimoto T, Araki Y, Akata S, Tokuuye K. Measuring hepatic functional reserve using low temporal resolution Gd-EOB-DTPA dynamic contrast-enhanced MRI: a preliminary study comparing galactosyl human serum albumin scintigraphy with indocyanine green retention. Eur Radiol. 2014;24(1):112-9.

55. Noren B, Forsgren MF, Dahlqvist Leinhard O, Dahlstrom N, Kihlberg J, Romu T, et al. Separation of advanced from mild hepatic fibrosis by quantification of the hepatobiliary uptake of Gd-EOB-DTPA. Eur Radiol. 2013;23(1):174-81.

56. Xie S, Sun Y, Wang L, Yang Z, Luo J, Wang W. Assessment of liver function and liver fibrosis with dynamic Gd-EOB-DTPA-enhanced MRI. Acad Radiol. 2015;22(4):460-6.

57. Juluru K, Talal AH, Yantiss RK, Spincemaille P, Weidman EK, Giambrone AE, et al. Diagnostic accuracy of intracellular uptake rates calculated using dynamic Gd-EOB-DTPA-enhanced MRI for hepatic fibrosis stage. J Magn Reson Imaging. 2017;45(4):1177-85.

58. Keller S, Sedlacik J, Schuler T, Buchert R, Avanesov M, Zenouzi R, et al. Prospective comparison of diffusion-weighted MRI and dynamic Gd-EOB-DTPA-enhanced MRI for detection and staging of hepatic fibrosis in primary sclerosing cholangitis. Eur Radiol. 2019;29(2):818-28.

59. Hoffman DH, Ayoola A, Nickel D, Han F, Chandarana H, Babb J, Shanbhogue KP. MR elastography, T1 and T2 relaxometry of liver: role in noninvasive assessment of liver function and portal hypertension. Abdom Radiol (NY). 2020;45(9):2680-7.

60. Allkemper T, Sagmeister F, Cicinnati V, Beckebaum S, Kooijman H, Kanthak C, et al. Evaluation of fibrotic liver disease with whole-liver T1rho MR imaging: a feasibility study at 1.5 T. Radiology. 2014;271(2):408-15.

61. Singh A, Reddy D, Haris M, Cai K, Rajender Reddy K, Hariharan H, Reddy R. T1rho MRI of healthy and fibrotic human livers at 1.5 T. J Transl Med. 2015;13:292.

62. Suyama Y, Tomita K, Soga S, Kuwamura H, Murakami W, Hokari R, Shinmoto H. T1rho magnetic resonance imaging value as a potential marker to assess the severity of liver fibrosis: A pilot study. Eur J Radiol Open. 2021;8:100321.

63. Xie S, Li Q, Cheng Y, Zhang Y, Zhuo Z, Zhao G, Shen W. Impact of Liver Fibrosis and Fatty Liver on T1rho Measurements: A Prospective Study. Korean J Radiol. 2017;18(6):898-905.

64. Hou J, Wong VW, Qian Y, Jiang B, Chan AW, Leung HH, et al. Detecting Early-Stage Liver Fibrosis Using Macromolecular Proton Fraction Mapping Based on Spin-Lock MRI: Preliminary Observations. J Magn Reson Imaging. 2023;57(2):485-92.

65. Yoshimaru D, Takatsu Y, Suzuki Y, Miyati T, Hamada Y, Funaki A, et al. Diffusion kurtosis imaging in the assessment of liver function: Its potential as an effective predictor of liver function. Br J Radiol. 2019;92(1094):20170608.

66. Jiang H, Chen J, Gao R, Huang Z, Wu M, Song B. Liver fibrosis staging with diffusion-weighted imaging: a systematic review and meta-analysis. Abdom Radiol (NY). 2017;42(2):490-501.

67. Emara DM, Reda MM, Elwazzan DA. Utility of diffusion weighted imaging (DWI) in assessment of liver fibrosis. D.M. Emara, Department of Radiology, Faculty of Medicine, Alexandria University, Egypt2018 2018.

68. Verloh N, Utpatel K, Haimerl M, Zeman F, Fellner C, Dahlke M, et al. DWI - histology: a possible means of determining degree of liver fibrosis? Oncotarget. 2018;9(28):20112-8.

69. Besheer T, Elalfy H, Abd El-Maksoud M, Abd El-Razek A, Taman S, Zalata K, et al. Diffusion-weighted magnetic resonance imaging and micro-RNA in the diagnosis of hepatic fibrosis in chronic hepatitis C virus. World J Gastroenterol. 2019;25(11):1366-77.

70. Charatcharoenwitthaya P, Sukonrut K, Korpraphong P, Pongpaibul A, Saiviroonporn P. Diffusion-weighted mag-

netic resonance imaging for the assessment of liver fibrosis in chronic viral hepatitis. PLoS One. 2021;16(3):e0248024.

71. Kahraman AS, Kahraman B, Ozdemir ZM, Karaca L, Sahin N, Yilmaz S. Diffusion-weighted imaging of the liver in assessing chronic liver disease: effects of fat and iron deposition on ADC values. Eur Rev Med Pharmacol Sci. 2022;26(18):6620-31.

72. Ozkurt H, Keskiner F, Karatag O, Alkim C, Erturk SM, Basak M. Diffusion Weighted MRI for Hepatic Fibrosis: Impact of b-Value2014 2014.

73. Zaiton F, Dawoud H, El Fiki IM, Hadhoud KM. Diffusion weighted MRI and transient elastography assessment of liver fibrosis in hepatitis C patients: Validity of non invasive imaging techniques. F. Zaiton, Radiology Department, Zagazig University, Moalemeen Division, Zagazig, Egypt2014 2014.

74. Fu F, Shi D, Zhu S, Wang M, Chen C, Li D, et al. Evaluation of hepatic fibrosis by using stretched-exponential and mono-exponential diffusion-weighted MR imaging. D. Shi, Departments of Radiology, The People's Hospital of Zhengzhou University & Henan Provincial People's Hospital, Zhengzhou, Henan, China2016 2016.

75. Papalavrentios L, Sinakos E, Chourmouzi D, Hytiroglou P, Drevelegas K, Constantinides M, et al. Value of 3 Tesla diffusion-weighted magnetic resonance imaging for assessing liver fibrosis2015 2015.

76. Yang ZX, Hu XX, Grimm R, Fu CX, Yan X, Zeng MS, Rao SX. Value of whole-liver apparent diffusion coefficient histogram analysis for quantification of liver fibrosis stages. S.-X. Rao, Department of Radiology, Zhongshan Hospital, Fudan University, and Shanghai Medical Imaging Institute, 180 Fenglin Rd., Shanghai, China2019 2019.

77. Abdelmaksoud AHK, El-Raziky M, El-Sayed M, Elsharkawy A, Ashour MK, Khattab H, Esmat G. Diffusion-weighted MRI and fibroscan vs. Histopathology for assessment of liver fibrosis in chronic HCV patients: (Pilot study). A.H.K. Abdelmaksoud, Diagnostic and Interventional Radiology Department, Faculty of Medicine, Cairo University, Egypt2015 2015.

78. Tokgoz O, Unal I, Turgut GG, Yildiz S. The value of liver and spleen ADC measurements in the diagnosis and follow up of hepatic fibrosis in chronic liver disease2014 2014.

79. Serag D, Ragab E. Diffusion-weighted MRI in staging of post hepatitis C fibrosis: does ADC value challenge liver biopsy? Egyptian Journal of Radiology and Nuclear Medicine. 2020;51(1):179.

80. Cece H, Ercan A, Yildiz S, Karakas E, Karakas O, Boyaci FN, et al. The use of DWI to assess spleen and liver quantitative ADC changes in the detection of liver fibrosis stages in chronic viral hepatitis2013 2013.

81. Amin MA, Eltomey MA, Abdelazeem MA, Yusif M. Diffusion weighted MRI in chronic viral hepatitis C: Correlation between apparent diffusion coefficient values and histopathological scores. M.A. Eltomey, Radiology and Imaging Department, Faculty of Medicine, Tanta University, Egypt2014 2014.

82. Bulow R, Mensel B, Meffert P, Hernando D, Evert M, Kuhn J-P. Diffusion-weighted magnetic resonance imaging for staging liver fibrosis is less reliable in the presence of fat and iron2013 2013.

83. Keller S, Sedlacik J, Schuler T, Buchert R, Avanesov M, Zenouzi R, et al. Prospective comparison of diffusion-weighted MRI and dynamic Gd-EOB-DTPA-enhanced MRI for detection and staging of hepatic fibrosis in primary sclerosing cholangitis2019 2019.

84. Shin MK, Song JS, Hwang SB, Hwang HP, Kim YJ, Moon WS. Liver Fibrosis Assessment with Diffusion-Weighted Imaging: Value of Liver Apparent Diffusion Coefficient Normalization Using the Spleen as a Reference Organ2019 2019.

85. Ye Z, Wei Y, Chen J, Yao S, Song B. Value of intravoxel incoherent motion in detecting and staging liver fibrosis: A meta-analysis. World J Gastroenterol. 2020;26(23):3304-17.

86. Ren H, Liu Y, Lu J, An W, Wang W, Yan T, et al. Evaluating the clinical value of MRI multi-model diffusion-weighted imaging on liver fibrosis in chronic hepatitis B patients2021 2021.

87. Tosun M, Onal T, Uslu H, Alparslan B, Akhan SC. Intravoxel incoherent motion imaging for diagnosing and staging the liver fibrosis and inflammation. Kocaeli Univ, Dept Radiol, Sch Med, Kocaeli, Turkey Kocaeli Univ, Dept Infect Dis & Clin Microbiol, Sch Med, Kocaeli, Turkey2020 2020.

88. Gulbay M, Ciliz DS, Celikbas AK, Ocalan DT, Sayin B, Ozbay BO, Alp E. Intravoxel incoherent motion parameters in the evaluation of chronic hepatitis B virus-induced hepatic injury: fibrosis and capillarity changes2020 2020.

89. Franca M, Marti-Bonmati L, Alberich-Bayarri A, Oliveira P, Guimaraes S, Oliveira J, et al. Evaluation of fibrosis and inflammation in diffuse liver diseases using intravoxel incoherent motion diffusion-weighted MR imaging. Abdom Radiol (NY). 2017;42(2):468-77.

90. Murphy P, Hooker J, Ang B, Wolfson T, Gamst A, Bydder M, et al. Associations between histologic features of nonalcoholic fatty liver disease (NAFLD) and quantitative diffusion-weighted MRI measurements in adults. Univ Calif San Diego, Dept Radiol, Liver Imaging Grp, San Diego, CA 92103 USA Univ Calif San Diego, Dept Med, Div Gastroenterol, NAFLD Translat Res Unit, San Diego, CA 92103 USA San Diego Supercomp Ctr, Computat & Appl Stat Lab, San Diego, CA USA Western Washington Pathol, Tacoma, WA USA Pacific Rim Pathol, San Diego, CA USA Univ Calif San Diego, Dept Family & Preventat Med, Div Epidemiol, San Diego, CA 92103 USA2015 2015.

91. Tosun M, Inan N, Sarisoy HT, Akansel G, Gumustas S, Gurbuz Y, Demirci A. Diagnostic performance of conventional diffusion weighted imaging and diffusion tensor imaging for the liver fibrosis and inflammation2013 2013.

92. Yang L, Rao S, Wang W, Chen C, Ding Y, Yang C, et al. Staging liver fibrosis with DWI: is there an added value for diffusion kurtosis imaging?2018 2018.

93. Park JH, Seo N, Chung YE, Kim SU, Park YN, Choi J-Y, et al. Noninvasive evaluation of liver fibrosis: comparison of the stretched exponential diffusion-weighted model to other diffusion-weighted MRI models and transient elastography2021 2021.

94. D Y, T M, Y S, Y H, N M, A F, et al. Diffusion kurtosis imaging with the breath-hold technique for staging hepatic fibrosis: A preliminary study. Magnetic resonance imaging. 2018;47:33-8.

95. Lee Y-S, Yoo YJ, Jung YK, Kim JH, Seo YS, Yim HJ, et al. Multiparametric MR Is a Valuable Modality for Evaluating Disease Severity of Nonalcoholic Fatty Liver Disease2020 2020.

96. Geethakumari P, Kampa P, Parchuri R, Bhandari R, Alnasser AR, Akram A, et al. Accuracy of Ultrasonography vs. Elastography in Patients With Non-alcoholic Fatty Liver Disease: A Systematic Review. Cureus. 2022;14(10):e29967.

97. Gu Q, Cen L, Lai J, Zhang Z, Pan J, Zhao F, et al. A meta-analysis on the diagnostic performance of magnetic resonance imaging and transient elastography in nonalcoholic fatty liver disease. Eur J Clin Invest. 2021;51(2):e13446.

98. Qu Y, Li M, Hamilton G, Zhang YN, Song B. Diagnos-

tic accuracy of hepatic proton density fat fraction measured by magnetic resonance imaging for the evaluation of liver steatosis with histology as reference standard: a meta-analysis. Eur Radiol. 2019;29(10):5180-9.

99. C B, A A, J J-Z, M F, B P, B C, et al. Quantification of steatosis in alcoholic and nonalcoholic fatty liver disease: Evaluation of four MR techniques versus biopsy. Ireland2019 2019-9. 169-74 p.

100. Wildman-Tobriner B, Middleton MM, Moylan CA, Rossi S, Flores O, Chang ZA, et al. Association Between Magnetic Resonance Imaging–Proton Density Fat Fraction and Liver Histology Features in Patients With Nonalcoholic Fatty Liver Disease or Nonalcoholic Steatohepatitis. B. Wildman-Tobriner, Duke University Medical Center, Department of Radiology, 2301 Erwin Road, Box 3808, Durham, NC, United States2018 2018.

101. Kim BK, Bernstein N, Huang DQ, Tamaki N, Imajo K, Yoneda M, et al. Clinical and histologic factors associated with discordance between steatosis grade derived from histology vs. MRI-PDFF in NAFLD. Aliment Pharmacol Ther. 2023;58(2):229-37.

102. Kang B-K, Kim M, Song S-Y, Jun DW, Jang K. Feasibility of modified Dixon MRI techniques for hepatic fat quantification in hepatic disorders: validation with MRS and histology2018 2018.

103. Kukuk GM, Hittatiya K, Sprinkart AM, Eggers H, Gieseke J, Block W, et al. Comparison between modified Dixon MRI techniques, MR spectroscopic relaxometry, and different histologic quantification methods in the assessment of hepatic steatosis2015 2015.

104. Choi SJ, Kim SM, Kim YS, Kwon OS, Shin SK, Kim KK, et al. Magnetic Resonance-Based Assessments Better Capture Pathophysiologic Profiles and Progression in Nonalcoholic Fatty Liver Disease2021 2021.

105. Imajo K, Kessoku T, Honda Y, Tomeno W, Ogawa Y, Mawatari H, et al. Magnetic Resonance Imaging More Accurately Classifies Steatosis and Fibrosis in Patients With Nonalcoholic Fatty Liver Disease Than Transient Elastography. Yokohama City Univ, Grad Sch Med, Dept Gastroenterol, Yokohama, Kanagawa 232, Japan Yokohama City Univ, Grad Sch Med, Dept Biostat & Epidemiol, Yokohama, Kanagawa 232, Japan Hiroshima Univ, Grad Sch Biomed Sci, Dept Med & Mol Sci, Hiroshima, Japan Kyoto Prefectural Univ Med, Dept Gastroenterol & Hepatol, Kamigyo Ku, Kyoto, Japan Kochi Med Sch, Dept Gastroenterol & Hepatol, Kochi, Japan Saga Med Sch, Div Hepatol, Ctr Liver, Saga, Japan Yokohama City Univ, Grad Sch Med, Dept Radiol, Yokohama, Kanagawa 232, Japan Shimane Univ, Fac Med, Dept Pharmacol, Izumo, Shimane, Japan2016 2016.

106. Shao CX, Ye J, Dong Z, Li F, Lin Y, Liao B, et al. Steatosis grading consistency between controlled attenuation parameter and MRI-PDFF in monitoring metabolic associated fatty liver disease2021 2021.

107. Clarke CN, Choi H, Hou P, Davis CH, Ma J, Rashid A, et al. Using MRI to non-invasively and accurately quantify preoperative hepatic steatosis2017 2017.

108. Cunha GM, Thai TT, Hamilton G, Covarrubias Y, Schlein A, Middleton MS, et al. Accuracy of common proton density fat fraction thresholds for magnitude- and complex-based chemical shift-encoded MRI for assessing hepatic steatosis in patients with obesity2020 2020.

109. Idilman IS, Keskin O, Elhan AH, Idilman R, Karcaaltincaba M. Impact of sequential proton density fat fraction for quantification of hepatic steatosis in nonalcoholic fatty liver disease2014 2014.

110. Idilman IS, Aniktar H, Idilman R, Kabacam G, Savas B, Elhan A, et al. Hepatic steatosis: quantification by proton density fat fraction with MR imaging versus liver biopsy2013 2013.

111. Jayakumar S, Middleton MS, Lawitz EJ, Mantry PS, Caldwell SH, Arnold H, et al. Longitudinal correlations between MRE, MRI-PDFF, and liver histology in patients with nonalcoholic steatohepatitis: Analysis of data from a phase II trial of selonsertib. Univ Calif San Diego, San Diego, CA 92103 USA Univ Texas Hlth San Antonio, Texas Liver Inst, San Antonio, TX USA Methodist Dallas, Liver Inst, Dallas, TX USA Univ Virginia, Charlottesville, VA USA Gastroenterol Consultants San Antonio, San Antonio, TX USA Duke Univ, Durham, NC USA Texas Clin Res Inst, Arlington, TX USA Toronto Liver Ctr, Toronto, ON, Canada Swedish Med Ctr, Seattle, WA USA Gilead Sci Inc, 353 Lakeside Dr, Foster City, CA 94404 USA Inova Fairfax Hosp, Falls Church, VA USA Harvard Med Sch, Beth Israel Deaconess Med Ctr, Boston, MA USA Univ Chicago, Chicago, IL 60637 USA2019 2019.

112. Beyer C, Hutton C, Andersson A, Imajo K, Nakajima A, Kiker D, et al. Comparison between magnetic resonance and ultrasound-derived indicators of hepatic steatosis in a pooled NAFLD cohort. A. Dennis, Perspectum, Oxford, United Kingdom2021 2021.

113. Hayashi T, Saitoh S, Takahashi J, Tsuji Y, Ikeda K, Kobayashi M, et al. Hepatic fat quantification using the two-point Dixon method and fat color maps based on nonalcoholic fatty liver disease activity score2017 2017.

114. Hu F, Yang R, Huang Z, Wang M, Yuan F, Xia C, et al. 3D Multi-Echo Dixon technique for simultaneous assessment of liver steatosis and iron overload in patients with chronic liver diseases: A feasibility study. B. Song, Department of Radiology, West China Hospital, Sichuan University, No. 37 Guoxue Alley, Wuhou District, Chengdu, China2019 2019.

115. Orcel T, Chau HT, Turlin B, Chaigneau J, Bannier E, Otal P, et al. Evaluation of proton density fat fraction (PDFF) obtained from a vendor-neutral MRI sequence and MRQuantif software2023 2023.

116. Benjamin H, Christian K, Stefan R, Robert E, Werner J, Heinz Z, et al. Evaluation of liver fat in the presence of iron with MRI using T2*correction: A clinical approach. H. Benjamin, Department of Radiology, Innsbruck Medical University, Anichstraße 35, 6020 Innsbruck, Austria2013 2013.

117. Liang J, Qiu B, Yin S, Chen Y, Zhang S. Predictive Value of Liver Stiffness Measurement by Magnetic Resonance Elastography for Complications after Liver Resection: A Systematic Review and Meta-Analysis. Digestion. 2022;103(5):357-66.

118. Cho HJ, Ahn YH, Sim MS, Eun JW, Kim SS, Kim BW, et al. Risk Prediction Model Based on Magnetic Resonance Elastography-Assessed Liver Stiffness for Predicting Posthepatectomy Liver Failure in Patients with Hepatocellular Carcinoma. Gut Liver. 2022;16(2):277-89.

119. Lee DH, Lee JM, Yi NJ, Lee KW, Suh KS, Lee JH, et al. Hepatic stiffness measurement by using MR elastography: prognostic values after hepatic resection for hepatocellular carcinoma. Eur Radiol. 2017;27(4):1713-21.

120. Lin H, Wang Y, Zhou J, Yang Y, Xu X, Ma D, et al. Tomoelastography based on multifrequency MR elastography predicts liver function reserve in patients with hepatocellular carcinoma: a prospective study2022 2022.

121. Selvaraj EA, Mozes FE, Jayaswal ANA, Zafarmand MH, Vali Y, Lee JA, et al. Diagnostic accuracy of elastog-

raphy and magnetic resonance imaging in patients with NAFLD: A systematic review and meta-analysis. J Hepatol. 2021;75(4):770-85.

122. Xu XY, Wang WS, Zhang QM, Li JL, Sun JB, Qin TT, Liu HB. Performance of common imaging techniques vs serum biomarkers in assessing fibrosis in patients with chronic hepatitis B: A systematic review and meta-analysis. World J Clin Cases. 2019;7(15):2022-37.

123. Xiao H, Shi M, Xie Y, Chi X. Comparison of diagnostic accuracy of magnetic resonance elastography and Fibroscan for detecting liver fibrosis in chronic hepatitis B patients: A systematic review and meta-analysis. PLoS One. 2017;12(11):e0186660.

124. Schambeck JPL, Forte GC, Goncalves LM, Stuker G, Kotlinski JBF, Tramontin G, et al. Diagnostic accuracy of magnetic resonance elastography and point-shear wave elastography for significant hepatic fibrosis screening: Systematic review and meta-analysis. PLoS One. 2023;18(2):e0271572.

125. Ooi GJ, Mgaieth S, Eslick GD, Burton PR, Kemp WW, Roberts SK, Brown WA. Systematic review and meta-analysis: non-invasive detection of non-alcoholic fatty liver disease related fibrosis in the obese. Obes Rev. 2018;19(2):281-94.

126. Hsu C, Caussy C, Imajo K, Chen J, Singh S, Kaulback K, et al. Magnetic Resonance vs Transient Elastography Analysis of Patients With Nonalcoholic Fatty Liver Disease: A Systematic Review and Pooled Analysis of Individual Participants. Clin Gastroenterol Hepatol. 2019;17(4):630-7 e8.

127. Duarte-Rojo A, Taouli B, Leung DH, Levine D, Nayfeh T, Hasan B, et al. Imaging-based non-invasive liver disease assessment for staging liver fibrosis in chronic liver disease: A systematic review supporting the AASLD Practice Guideline. Hepatology. 2024.

128. Dong B, Lyu G, Chen Y, Lin G, Wang H, Qin R, Gu J. Comparison of two-dimensional shear wave elastography, magnetic resonance elastography, and three serum markers for diagnosing fibrosis in patients with chronic hepatitis B: a meta-analysis. Expert Rev Gastroenterol Hepatol. 2021;15(9):1077-89.

129. Bi J, Liu L, Qin T. Comparison of magnetic resonance elastography and transient elastography in the diagnosis of hepatic fibrosis: a systematic review and meta-analysis. Ann Palliat Med. 2021;10(8):8692-700.

130. Besutti G, Valenti L, Ligabue G, Bassi MC, Pattacini P, Guaraldi G, Giorgi Rossi P. Accuracy of imaging methods for steatohepatitis diagnosis in non-alcoholic fatty liver disease patients: A systematic review. Liver Int. 2019;39(8):1521-34.

131. Zhang YN, Fowler KJ, Boehringer AS, Montes V, Schlein AN, Covarrubias Y, et al. Comparative diagnostic performance of ultrasound shear wave elastography and magnetic resonance elastography for classifying fibrosis stage in adults with biopsy-proven nonalcoholic fatty liver disease2022 2022.

132. Yoon JH, Lee JM, Joo I, Lee ES, Sohn JY, Jang SK, et al. Hepatic fibrosis: prospective comparison of MR elastography and US shear-wave elastography for evaluation2014 2014.

133. Yin M, Glaser KJ, Talwalkar JA, Chen J, Manduca A, Ehman RL. Hepatic MR Elastography: Clinical Performance in a Series of 1377 Consecutive Examinations2016 2016.

134. Wang J, Malik N, Yin M, Smyrk TC, Czaja AJ, Ehman RL, Venkatesh SK. Magnetic resonance elastography is accurate in detecting advanced fibrosis in autoimmune hepatitis2017 2017.

135. Shen P, Ma S, Xu H, Yang L, Zhu M, Qiu S, et al. A study of diagnostic performance of MR elastography in liver fibrosis with chronic hepatitis B. C. Hu, Department of Radiology, The First Affiliated Hospital of Soochow University, Suzhou, China2019 2019.

136. Chou C-T, Chen R-C, Wu W-P, Lin P-Y, Chen Y-L. Prospective Comparison of the Diagnostic Performance of Magnetic Resonance Elastography with Acoustic Radiation Force Impulse Elastography for Pre-operative Staging of Hepatic Fibrosis in Patients with Hepatocellular Carcinoma2017 2017.

137. Dyvorne HA, Jajamovich GH, Bane O, Fiel MI, Chou H, Schiano TD, et al. Prospective comparison of magnetic resonance imaging to transient elastography and serum markers for liver fibrosis detection. B. Taouli, Department of Radiology and Translational and Molecular Imaging Institute, Icahn School of Medicine at Mount Sinai, 1470 Madison Ave, New York, NY, United States2016 2016.

138. Tamaki N, Imajo K, Sharpton S, Jung J, Kawamura N, Yoneda M, et al. Magnetic resonance elastography plus Fibrosis-4 versus FibroScan–aspartate aminotransferase in detection of candidates for pharmacological treatment of NASH-related fibrosis. R. Loomba, NAFLD Research Center, Division of Gastroenterology and Hepatology, Department of Medicine, University of California San Diego, La Jolla, CA, United States2022 2022.

139. Lara Romero C, Liang J-X, Fernandez Lizaranzazu I, Ampuero Herrojo J, Castell J, Del Prado Alba C, et al. Liver stiffness accuracy by magnetic resonance elastography in histologically proven non-alcoholic fatty liver disease patients: a Spanish cohort2023 2023.

140. Wu WP, Chou CT, Chen RC, Lee CW, Lee KW, Wu HK. Non-invasive evaluation of hepatic fibrosis: The diagnostic performance of magnetic resonance elastography in patients with viral hepatitis B or C2015 2015.

141. Osman KT, Maselli DB, Idilman IS, Rowan DJ, Viehman JK, Harmsen WS, et al. Liver Stiffness Measured by Either Magnetic Resonance or Transient Elastography Is Associated with Liver Fibrosis and Is an Independent Predictor of Outcomes among Patients with Primary Biliary Cholangitis. J.E. Eaton, Medicine, Division of Gastroenterology and Hepatology, Mayo Clinic, 200 First Street South West, Rochester, MN, United States2021 2021.

142. Forsgren MF, Nasr P, Karlsson M, Dahlstrom N, Noren B, Ignatova S, et al. Biomarkers of liver fibrosis: prospective comparison of multimodal magnetic resonance, serum algorithms and transient elastography2020 2020.

143. DH H, A A, D N, F H, H C, J B, KP S. MR elastography, T1 and T2 relaxometry of liver: role in noninvasive assessment of liver function and portal hypertension. Abdominal radiology (New York). 2020;45(9):2680-7.

144. Leitao HS, Doblas S, Garteiser P, d'Assignies G, Paradis V, Mouri F, et al. Hepatic Fibrosis, Inflammation, and Steatosis: Influence on the MR Viscoelastic and Diffusion Parameters in Patients with Chronic Liver Disease. Univ Paris Diderot, Beaujon Hosp, AP HP,Sorbonne Paris Cite,UMR1149,INSERM, Lab Imaging Biomarkers,Ctr Res Inflammat,Dept Rad, 100 Blvd Gen Leclerc, F-92118 Clichy, France2017 2017.

145. Gharib AM, Han MAT, Meissner EG, Kleiner DE, Zhao X, McLaughlin M, et al. Magnetic resonance elastography shear wave velocity correlates with liver fibrosis and hepatic venous pressure gradient in adults with advanced liver disease. C.G. Morse, Critical Care Medicine Department, NIH Clinical Center, AIDS Section, Bethesda, MD, United States2017 2017.

146. Zhan C, Kannengiesser S, Chandarana H, Fenchel M, Ream J, Shanbhogue KP. MR elastography of liver at 3 Tesla: comparison of gradient-recalled echo (GRE) and spin-echo (SE) echo-planar imaging (EPI) sequences and agreement across stiffness measurements2019 2019.

147. Sofue K, Onoda M, Tsurusaki M, Morimoto D, Yada N, Kudo M, Murakami T. Dual-frequency MR elastography to differentiate between inflammation and fibrosis of the liver: Comparison with histopathology. Kobe Univ, Dept Radiol, Sch Med, Kobe, Hyogo, Japan Kindai Univ, Dept Radiol, Fac Med, Osaka, Japan Kindai Univ Hosp, Dept Radiol Technol, Osaka, Japan Kanazawa Univ, Grad Sch Med Sci, Div Hlth Sci, Kanazawa, Ishikawa, Japan Kindai Univ, Dept Gastroenterol & Hepatol, Fac Med, Osaka, Japan2020 2020.

148. Li M, Yang H, Liu Y, Zhang L, Chen J, Deng Y, et al. Comparison of the diagnostic performance of 2D and 3D MR elastography in staging liver fibrosis2021 2021.

149. Shi Y, Qi Y-F, Lan G-Y, Wu Q, Ma B, Zhang X-Y, et al. Three-dimensional MR Elastography Depicts Liver Inflammation, Fibrosis, and Portal Hypertension in Chronic Hepatitis B or C2021 2021.

150. Chen J, Allen AM, Therneau TM, Chen J, Li JH, Hoodeshenas S, et al. Liver stiffness measurement by magnetic resonance elastography is not affected by hepatic steatosis. Sichuan Univ, West China Hosp, Dept Radiol, 37 Guoxue Alley, Chengdu 610041, Peoples R China Mayo Clin, Dept Radiol, 200 First St SW, Rochester, MN 55905 USA Mayo Clin, Div Gastroenterol & Hepatol, 200 First St SW, Rochester, MN 55905 USA Mayo Clin, Div Biomed Stat & Informat, 200 First St SW, Rochester, MN 55905 USA2022 2022.

151. Troelstra MA, Witjes JJ, van Dijk A-M, Mak AL, Gurney-Champion O, Runge JH, et al. Assessment of Imaging Modalities Against Liver Biopsy in Nonalcoholic Fatty Liver Disease: The Amsterdam NAFLD-NASH Cohort2021 2021.

152. Feier D, Balassy C, Bastati N, Fragner R, Wrba F, Ba-Ssalamah A. The diagnostic efficacy of quantitative liver MR imaging with diffusion-weighted, SWI, and hepato-specific contrast-enhanced sequences in staging liver fibrosis—a multiparametric approach. A. Ba-Ssalamah, Department of Biomedical Imaging and Image-guided Therapy, Medical University of Vienna, General Hospital of Vienna (AKH), Waehringer Guertel 18-20, Vienna, Austria2016 2016.

153. Banerjee R, Pavlides M, Tunnicliffe EM, Piechnik SK, Sarania N, Philips R, et al. Multiparametric magnetic resonance for the non-invasive diagnosis of liver disease. J Hepatol. 2014;60(1):69-77.

154. McDonald N, Eddowes PJ, Hodson J, Semple SIK, Davies NP, Kelly CJ, et al. Multiparametric magnetic resonance imaging for quantitation of liver disease: a two-centre cross-sectional observational study2018 2018.

155. Mole DJ, Fallowfield JA, Sherif AE, Kendall T, Semple S, Kelly M, et al. Quantitative magnetic resonance imaging predicts individual future liver performance after liver resection for cancer. PLoS One. 2020;15(12):e0238568.

156. Unal E, Akata D, Karcaaltincaba M. Liver Function Assessment by Magnetic Resonance Imaging. Semin Ultrasound CT MR. 2016;37(6):549-60.

157. Breit HC, Block KT, Winkel DJ, Gehweiler JE, Henkel MJ, Weikert T, et al. Evaluation of liver fibrosis and cirrhosis on the basis of quantitative T1 mapping: Are acute inflammation, age and liver volume confounding factors? H.C. Breit, University Hospital Basel, University of Basel Clinic of Radiology & Nuclear Medicine, Petersgraben 4, Basel, Switzerland2021 2021.

158. Ocal O, Peynircioglu B, Loewe C, van Delden O, Vandecaveye V, Gebauer B, et al. Correlation of liver enhancement in gadoxetic acid-enhanced MRI with liver functions: a multicenter-multivendor analysis of hepatocellular carcinoma patients from SORAMIC trial2022 2022.

159. Wang C, Yuan XD, Wu N, Sun WR, Tian Y. Optimization of hepatobiliary phase imaging in gadoxetic acid-enhanced magnetic resonance imaging: a narrative review. Quant Imaging Med Surg. 2023;13(3):1972-82.

160. Ozturk A, Olson MC, Samir AE, Venkatesh SK. Liver fibrosis assessment: MR and US elastography. Abdom Radiol (NY). 2022;47(9):3037-50.

161. Yin M, Venkatesh SK. Ultrasound or MR elastography of liver: which one shall I use? Abdom Radiol (NY). 2018;43(7):1546-51.

162. Ghoz HM, Kroner PT, Stancampiano FF, Bowman AW, Vishnu P, Heckman MG, et al. Hepatic iron overload identified by magnetic resonance imaging-based T2* is a predictor of non-diagnostic elastography. Quant Imaging Med Surg. 2019;9(6):921-7.

163. Curtis WA, Fraum TJ, An H, Chen Y, Shetty AS, Fowler KJ. Quantitative MRI of Diffuse Liver Disease: Current Applications and Future Directions. Radiology. 2019;290(1):23-30.